

Dark matter allowed scenarios for Yukawa-unified $SO(10)$ SUSY GUTs

Howard Baer^a, Sabine Kraml^b, Sezen Sekmen^c and Heaya Summy^a

^a *Department of Physics, Florida State University Tallahassee, FL 32306, USA*

^b *Laboratoire de Physique de Subatomique et de Cosmologie, UJF Grenoble 1, CNRS/IN2P3, INPG, 53 Avenue des Martyrs, F-38026 Grenoble, France*

^c *Dept. of Physics, Middle East Technical Univ., TR-06531 Ankara, Turkey*
E-mail: baer@hep.fsu.edu, sabine.kraml@cern.ch, sezen.sekmen@cern.ch, heaya@hep.fsu.edu,

ABSTRACT: Simple supersymmetric grand unified models based on the gauge group $SO(10)$ require –in addition to gauge and matter unification– the unification of t – b – τ Yukawa couplings. Owing to sparticle contributions to fermion self-energy diagrams, the Yukawa unification however only occurs for very special values of the soft SUSY breaking parameters. We perform a search using a Markov Chain Monte Carlo (MCMC) technique to investigate model parameters and sparticle mass spectra which occur in Yukawa-unified SUSY models, where we also require the relic density of neutralino dark matter to saturate the WMAP-measured abundance. For Yukawa unified models with $\mu > 0$, the spectrum is characterized by three mass scales: first and second generation scalars in the multi-TeV range, third generation scalars in the TeV range, and gauginos in the ~ 100 GeV range. Most solutions give far too high a relic abundance of neutralino dark matter. The dark matter discrepancy can be rectified by *i*). allowing for neutralino decay to axino plus photon, *ii*). imposing gaugino mass non-universality or *iii*). imposing generational non-universality. In addition, the MCMC approach finds a compromise solution where scalar masses are not too heavy, and where neutralino annihilation occurs via the light Higgs h resonance. By imposing weak scale Higgs soft term boundary conditions, we are also able to generate low μ , m_A solutions with neutralino annihilation via a light A resonance, though these solutions seem to be excluded by CDF/D0 measurements of the $B_s \rightarrow \mu^+ \mu^-$ branching fraction. Based on the dual requirements of Yukawa coupling unification and dark matter relic density, we predict new physics signals at the LHC from pair production of 350–450 GeV gluinos. The events are characterized by very high b -jet multiplicity and a dilepton mass edge around $m_{\tilde{\chi}_2^0} - m_{\tilde{\chi}_1^0} \sim 50$ –75 GeV.

KEYWORDS: Supersymmetry Phenomenology, Supersymmetric Standard Model, Dark Matter.

Contents

1. Introduction	1
2. Random scan in HS model	6
2.1 Random scan results	7
2.2 Three proposals to reconcile Yukawa-unified models with dark matter relic density	11
2.2.1 Dark matter solution via neutralino decay to axino	11
2.2.2 Dark matter solution via non-universal gaugino masses	12
2.2.3 Dark matter solution via generational non-universality	13
3. Markov Chain Monte Carlo analysis	15
3.1 HS model: neutralino annihilation via h resonance	16
3.2 Solutions using weak scale Higgs boundary conditions	22
4. Yukawa-unified benchmark scenarios and LHC signatures	29
5. Summary and conclusions	32

1. Introduction

Grand unified theories (GUTs) based upon the gauge group $SO(10)$ certainly have to be considered as among the most beautiful ideas in particle physics [1]. In addition to gauge group unification, one also has matter unification of each generation within the $SO(10)$ 16-dimensional spinorial representation $\psi(16)$. Furthermore, the simplest $SO(10)$ GUT theories also allow for Yukawa coupling unification. The ad-hoc but fortuitous triangle anomaly cancellation found in the SM or even $SU(5)$ GUTs is a simple mathematical fact in $SO(10)$. The beauty of $SO(10)$ is only enhanced via a marriage to softly broken $N = 1$ supersymmetry (SUSY), which stabilizes the gauge hierarchy, and is experimentally supported by gauge coupling unification found within the MSSM (provided superpartners exist at or around the weak scale). SUSY $SO(10)$ also elegantly addresses the neutrino mass problem, since one only has matter unification within the superfield $\hat{\psi}(16)$ provided one introduces an additional (SM gauge singlet) superfield \hat{N}^c which contains a right-handed neutrino state. Under the breaking of $SO(10)$, a superpotential term leading to a Majorana mass is allowed for the \hat{N}^c field; this naturally yields a description of neutrino masses in terms of the elegant see-saw mechanism [3].

Standard GUTs and also SUSYGUTs formulated in 4-d spacetime have fallen into disrepute due to a variety of problems associated with GUT gauge symmetry breaking via the Higgs mechanism. These include the doublet-triplet splitting problem, lack of observation of proton decay, and the frequently awkward implementation of GUT symmetry breaking via at least one large and unwieldy Higgs representation. With the onset of model building utilizing extra dimensions, it has been shown to be possible to formulate SUSYGUTs in 5 or more spacetime dimensions. Then, the GUT gauge symmetry can be broken via

compactification of the extra dimensions on a suitable sub-space, such as an orbifold. In these 5-d and 6-d SUSYGUT models, the large GUT scale Higgs representations can be dispensed with, the doublet-triplet splitting problem can be solved, and the proton can be made longer-lived than current limits or even absolutely stable [2]. The extra-dimensional SUSYGUT models act as a sort of “proof of principle” of what might be possible in more complicated set-ups where the SUSYGUT model might arise from compactification of superstring models.

The imminent turn-on of the CERN LHC naturally leads one to ask: How might $SO(10)$ SUSYGUT theories manifest themselves in the environment of an LHC detector? Our goal in this paper is to address this question. To do so, our path will be guided by the twin requirements of *i*). Yukawa coupling unification and *ii*). explaining the measured dark matter (DM) abundance of the universe. Our answer we find is that, if DM-allowed, Yukawa-unified $SO(10)$ SUSYGUTs are correct, then we expect new physics at LHC to consist of gluino pair production events with $m_{\tilde{g}} \sim 350\text{--}450$ GeV, followed by 3-body gluino cascade decays to b -jet rich final states. In addition, an opposite sign/same-flavor (OS/SF) isolated dilepton invariant mass spectrum should have a mass edge at around 50–75 GeV. SUSY scalar fields other than the light Higgs h are very heavy, and largely decouple from LHC physics. The remainder of this paper details our methodology as to how we come to these conclusions.

In this paper, we assume nature is described by an $SO(10)$ SUSYGUT theory at energy scales $Q > M_{GUT} \sim 2 \times 10^{16}$ GeV. We further assume that the $SO(10)$ SUSYGUT model breaks (either via the Higgs mechanism or via compactification of extra dimensions) to the MSSM (or MSSM plus right-handed neutrino states) at $Q = M_{GUT}$. Thus, below M_{GUT} , the MSSM is the correct effective field theory which describes nature. We will further assume that the superpotential above M_{GUT} is of the form

$$\hat{f} \ni f \hat{\psi}_{16} \hat{\psi}_{16} \hat{\phi}_{10} + \cdots \quad (1.1)$$

so that the three third generation Yukawa couplings f_t , f_b and f_τ are unified at M_{GUT} . It is simple in this context to include as well the effect of a third generation neutrino Yukawa coupling f_ν ; this effect has been shown to be small, although it can help improve Yukawa coupling unification by a few per cent if the neutrino Majorana mass scale is within a few orders of magnitude of M_{GUT} . Within this ansatz, the GUT scale soft SUSY breaking (SSB) terms are constrained by the $SO(10)$ gauge symmetry so that matter scalar SSB terms have a common mass m_{16} , Higgs scalar SSB terms have a common mass m_{10} and there is a common trilinear soft breaking parameter A_0 . As usual, the bilinear soft term B can be traded for $\tan\beta$, the ratio of Higgs field vevs, while the magnitude of the superpotential Higgs mass μ is determined in terms of M_Z^2 via the electroweak symmetry breaking minimization conditions. Here, electroweak symmetry is broken radiatively (REWSB) due to the large top quark mass. In order to accomodate REWSB, it is well-known that in Yukawa-unified models, the GUT scale Higgs soft masses must be *split* such that $m_{H_u}^2 < m_{H_d}^2$ in order to fulfill the EWSB minimization conditions; this effectively gives $m_{H_u}^2$ a head start over $m_{H_d}^2$ in running towards negative values at or around the weak scale. We parametrize the Higgs splitting as $m_{H_{u,d}}^2 = m_{10}^2 \mp 2M_D^2$. The Higgs mass splitting might originate via a large

near-GUT-scale threshold correction arising from the neutrino Yukawa coupling: see the Appendix to Ref. [4] for discussion. Thus, the Yukawa unified SUSY model is determined by the parameter space

$$m_{16}, m_{10}, M_D^2, m_{1/2}, A_0, \tan\beta, \text{sign}(\mu) \quad (1.2)$$

along with the top quark mass. We will take $m_t = 171$ GeV, in accord with recent measurements from CDF and D0 [5].

Much previous work has been done on the topic of t - b - τ unification in $SO(10)$ SUSYGUTs. Early on it was found that t - b - τ Yukawa unification could only occur at very high values of $\tan\beta$ [6]. The importance of weak scale MSSM threshold corrections to fermion masses was noted by Hall, Rattazzi and Sarid[8]. It was also noted that with Yukawa coupling unification, in order to obtain an appropriate REWSB, the GUT scale Higgs masses would need to be split such that $m_{H_u}^2 < m_{H_d}^2$ —perhaps via D -term contributions[9] to *all* scalar masses (the DT model), or via splitting of *only* the Higgs soft terms[4] (the HS model).

In Ref. [10], it was found using the Isajet sparticle mass spectrum generator [11] Isasuga that Yukawa coupling unification to 5% could be achieved in the MSSM using D -term splitting, but only for $\mu < 0$; for $\mu > 0$, the Yukawa coupling unification was much worse, of order 30–50%. These parameter space scans allowed m_{16} values up to only 1.5 TeV, and used a GUT scale Yukawa unification quantity

$$R = \frac{\max(f_t, f_b, f_\tau)}{\min(f_t, f_b, f_\tau)}, \quad (1.3)$$

so that *e.g.* $R = 1.1$ would correspond to 10% Yukawa unification. The $\mu < 0$ Yukawa unification solutions were examined in more detail in Ref. [12], where dark matter allowed solutions were found, and the neutralino A -annihilation funnel was displayed for the first time.

With the announcement from BNL experiment E-821 that there was a 3σ deviation from SM predictions on the muon anomalous magnetic moment $a_\mu \equiv (g-2)_\mu/2$, attention shifted back to $\mu > 0$ solutions. Ref. [13], using the DT model with parameter space scans of m_{16} up to 2 TeV, found Yukawa-unified solutions with $R \sim 1.3$ but only for special choices of GUT scale boundary conditions:

$$A_0 \sim -2m_{16}, \quad m_{10} \sim 1.2m_{16}, \quad (1.4)$$

with $m_{1/2} \ll m_{16}$ and $\tan\beta \sim 50$. In fact, these boundary conditions had been found earlier by Bagger *et al.* [14] in the context of models with a *radiatively driven inverted scalar mass hierarchy* (RIMH), wherein RG running of multi-TeV GUT scale scalar masses caused third generation masses to be driven to weak scale values, while first/second generation soft terms remained in the multi-TeV regime. These models, which required Yukawa coupling unification, were designed to maintain low fine-tuning by having light third generation scalars, while solving the SUSY flavor and CP problems via multi-TeV first and second generation scalars. A realistic implementation of these models in Ref. [15] using 2-loop RGEs and requiring REWSB found that an inverted hierarchy could be generated, but

only to a lesser extent than that envisioned in Ref. [14], which didn't implement EWSB or calculate an actual physical mass spectrum.

Simultaneously with Ref. [13], Blazek, Dermisek and Raby (BDR) published results showing Yukawa-unified solutions using the HS model solution [4]. Their results *also* found valid solutions using the Bagger *et al.* boundary conditions. BDR used a top-down method beginning with actual Yukawa unification at M_{GUT} , and implemented 2-loop gauge and Yukawa running but 1-loop soft term running. They extracted physical soft terms at scale $Q = M_Z$, and minimized a two-Higgs doublet scalar potential to achieve REWSB, also at scale M_Z . Each run generated a numerical value for third generation t , b and τ masses and other electroweak and QCD observables. A χ^2 fit was performed to select those solutions which best matched the measured weak scale fermion masses and other parameters. BDR scanned m_{16} values up to 2 TeV, and found best fit results with $m_A \sim 100$ GeV and $\mu \sim 100$ –200 GeV, in contrast to Ref. [13], where solutions with valid EWSB could only be found if $\mu \sim m_A \sim m_{\tilde{t}_1} \sim 1$ TeV.¹

In a long follow-up study using Isajet, Auto *et al.* [18] found that Yukawa-unified solutions good to less than a few percent could be found in the $\mu > 0$ case using the HS model of BDR, but only for very large values of $m_{16} \gtrsim 5$ –10 TeV and low values of $m_{1/2} \lesssim 100$ GeV, again using Bagger *et al.* boundary conditions. Yukawa unification in the DT model was at best good to 10% (for this reason, in the present paper we will focus only on the HS model). The spectra were characterized by three mass scales:

1. ~ 5 –15 TeV first and second generation scalars,
2. ~ 1 TeV third generations scalars, μ term and m_A and
3. chargino masses $m_{\tilde{\chi}_1^\pm} \sim 100$ –200 GeV and gluino masses $m_{\tilde{g}} \sim 350$ –450 GeV.

These Yukawa-unified solutions—owing to very large values of scalar masses, m_A and μ —predicted dark matter relic density values $\Omega_{\tilde{\chi}_1^0} h^2$ far beyond the WMAP-measured result [19] of

$$\Omega_{\text{DM}} h^2 = 0.111_{-0.015}^{+0.011} \quad (2\sigma). \quad (1.5)$$

Meanwhile, the spectra generated using the BDR program could easily generate $\Omega_{\tilde{\chi}_1^0} h^2$ values close to 0.1 since their allowed μ and m_A values were far lower, so that mixed higgsino dark matter or A -funnel annihilation solutions could easily be found. In follow-up papers to the BDR program [20, 21], the neutralino relic density and branching fraction $B_s \rightarrow \mu^+ \mu^-$ were evaluated. To avoid constraints on $BF(B_s \rightarrow \mu^+ \mu^-)$ from the CDF collaboration, the best fit values of m_{16} and m_A have been steadily increasing, so that the latest papers have $m_A \sim 500$ GeV and $m_{16} \sim 3$ TeV, while μ can still be of order 100 GeV [21]. In Ref. [22], attempts were made to reconcile the Isajet Yukawa-unified solutions with the dark matter relic density. The two solutions advocated were 1. lowering GUT scale first/second generation scalars relative to the third, to gain neutralino-squark

¹A paper by Tobe and Wells[16] (TW) appeared after Ref. [4]. While TW calculate no actual spectra or address EWSB, they do adopt a semi-model independent approach which favors $t - b - \tau$ Yukawa coupling unification if scalar masses are in the multi-TeV regime while gauginos are as light as possible.

or neutralino-slepton co-annihilation solutions [23], or 2. increasing the GUT scale gaugino mass M_1 , so the relic density could be lowered by bino-wino co-annihilation [24].

In this paper, we report on a new examination of SUSY mass spectra constrained by Yukawa coupling unification. We are motivated by the following rationale.

- We use the latest measured value of the top quark mass— $m_t = 171$ GeV [5]— whereas earlier analyses used $m_t = 175$ GeV or even higher values.
- We generate SUSY mass spectra using Isajet 7.75, which includes several upgrades to the SUSY spectrum calculation from versions used in earlier analyses [25].
- We use a Markov Chain Monte Carlo (MCMC) technique, which is much more efficient at searching through multi-dimensional parameter spaces.
- We adopt an alternative approach to implementing Higgs sector SSB boundary conditions, which simultaneously imposes GUT-scale Higgs (GSH) and weak-scale Higgs (WSH) soft term boundary conditions. This allows us to explore solutions akin to those found by BDR with low values of m_A and μ . These solutions are difficult to generate using a purely top-down approach, due to a high degree of fine-tuning in the EWSB sector.

In Sections 2 and 3, we present results from our calculations. These include:

1. A variety of solutions consistent with Ref. [18] with very large values of $m_{16} \sim 5\text{--}15$ TeV, and very light gauginos. These solutions always have *too large* a dark matter relic density. We propose they may still be valid by invoking an unstable lightest neutralino which decays to an *axino* lightest SUSY particle (LSP).
2. New solutions are found with $m_{16} \sim 3$ TeV and $m_{1/2} \sim 100$ GeV with Yukawa unification to $\sim 8\%$, but with a valid relic density due to neutralino annihilation through the light Higgs h resonance.
3. Using simultaneous GSH and WSH boundary conditions, we are able to generate BDR-like solutions using Isajet with $m_{16} \sim 3\text{--}7$ TeV but with $m_{1/2} \sim 100\text{--}400$ GeV with good relic density due to neutralino annihilation through the pseudoscalar Higgs A resonance. The A -resonance annihilation solutions have excellent Yukawa unification, but with $m_A \sim 150\text{--}230$ GeV and $\tan \beta \sim 50$, are all excluded by measurements of the $B_s \rightarrow \mu^+ \mu^-$ branching fraction. Solutions with higher m_A and low μ with mixed higgsino dark matter also can be found, but tend to have Yukawa unification $R > 1.2$.
4. We also re-examine the first class of solutions, but solving the DM problem via generational non-universality or gaugino mass non-universality, as in Ref. [22].

In Sec. 4, we discuss a Table of benchmark scenarios for each of these cases. The cases are suitable for collider event generation. We also discuss implications of each of these scenarios for collider searches at the CERN LHC.

Our preferred solutions— numbers 1. and 2. above— lead to spectra with first/second generation scalar masses in the 3 – 15 TeV range, while gluino masses are in the 350 – 450 GeV range. (Solution number 3 is likely ruled out by the measured limit on $BF(B_s \rightarrow \mu^+ \mu^-)$ and solution 4 gives up either gaugino mass unification or generational unification.) Thus, we predict that DM-allowed Yukawa-unified $SO(10)$ SUSY GUT models will lead to collider events at the CERN LHC typified by nearly pure gluino pair production followed by cascade decays $\tilde{g} \rightarrow t b \tilde{\chi}_1^\pm$, $b \bar{b} \tilde{\chi}_2^0$ and $b \bar{b} \tilde{\chi}_1^0$. The gluino pair events will occur with cross sections in the $\sim 10^5$ fb range, and will be very rich in b -jets. There should exist a characteristic OS/SF dilepton mass edge at $m_{\tilde{\chi}_2^0} - m_{\tilde{\chi}_1^0} \sim 50\text{--}75$ GeV.

A summary and conclusions are presented in Sec. 5.

2. Random scan in HS model

In this section, we explore the parameter space Eq. (1.2) for Yukawa-unified solutions by means of a random scan. We wish to first check and update results presented in Ref. [18], using the latest Isajet version and a top quark mass of $m_t = 171$ GeV in accord with recent measurements from the Fermilab Tevatron [5]. The degree of Yukawa unification, R , is defined in Eq. (1.3), so that *e.g.* a value of $R = 1.1$ corresponds to 10% Yukawa unification.

For our calculations, we adopt the Isajet 7.75 [11, 25] SUSY spectrum generator Isasugra. Isasugra begins the calculation of the sparticle mass spectrum with input \overline{DR} gauge couplings and f_b, f_τ Yukawa couplings at the scale $Q = M_Z$ (f_t running begins at $Q = m_t$) and evolves the 6 couplings up in energy to scale $Q = M_{GUT}$ (defined as the value Q where $g_1 = g_2$) using two-loop RGEs.² At $Q = M_{GUT}$, the SSB boundary conditions are input, and the set of 26 coupled two-loop MSSM RGEs [27] are used to evolve couplings and SSB terms back down in scale to $Q = M_Z$. Full two-loop MSSM RGEs are used for soft term evolution, while the gauge and Yukawa coupling evolution includes threshold effects in the one-loop beta-functions, so the gauge and Yukawa couplings transition smoothly from the MSSM to SM effective theories as different mass thresholds are passed. In Isajet 7.75, the SSB terms of sparticles which mix are frozen out at the scale $Q \equiv M_{SUSY} = \sqrt{\tilde{m}_{t_L} \tilde{m}_{t_R}}$, while non-mixing SSB terms are frozen out at their own mass scale [25]. The scalar potential is minimized using the RG-improved one-loop MSSM effective potential evaluated at an optimized scale $Q = M_{SUSY}$ which accounts for leading two-loop effects [28]. Once the tree-level sparticle mass spectrum is computed, full one-loop radiative corrections are calculated for all sparticle and Higgs boson masses, including complete one-loop weak scale threshold corrections for the top, bottom and tau masses at scale $Q = M_{SUSY}$. These fermion self-energy terms are critical to evaluating whether or not Yukawa couplings do indeed unify. Since the GUT scale Yukawa couplings are modified by the threshold corrections, the Isajet RGE solution must be imposed iteratively with successive up-down running until a convergent solution for the spectrum is found. For most of parameter

²As inputs, we take the top quark pole mass $m_t = 171$ GeV. We also take $m_b^{\overline{DR}}(M_Z) = 2.83$ GeV [26] and $m_\tau^{\overline{DR}}(M_Z) = 1.7463$ GeV. The paper Ref. [18] addresses consequences of varying the values of m_t and m_b .

space, there is very good agreement between Isajet and the other public spectrum codes SoftSusy, SuSpect and SPheno, although at the edges of parameter space agreement between the four codes typically diminishes [29].

We first adopt a wide parameter range scan, and then once the best Yukawa-unified regions are found, we adopt a narrow scan to try to hone in on the best unified solutions. The parameter range we adopt for the wide (narrow) scan is

$$\begin{aligned}
m_{16} : & \quad 0 - 20 \text{ TeV} & (1 - 20 \text{ TeV}), \\
m_{10}/m_{16} : & \quad 0 - 1.5 & (0.8 - 1.4), \\
m_{1/2} : & \quad 0 - 5 \text{ TeV} & (0 - 1 \text{ TeV}), \\
A_0/m_{16} & \quad -3 - 3 & (-2.5 - 1.9), \\
M_D/m_{16} : & \quad 0 - 0.8 & (0.25 - 0.8), \\
\tan \beta : & \quad 40 - 60 & (46 - 53).
\end{aligned} \tag{2.1}$$

For the random scan, we evaluate $\Omega_{\tilde{\chi}_1^0} h^2$, $BF(b \rightarrow s\gamma)$, Δa_μ and $BF(B_S \rightarrow \mu^+ \mu^-)$ using Isatools (a sub-package of Isajet). We plot only solutions for which $m_{\tilde{\chi}_1^\pm} > 103.5 \text{ GeV}$, in accord with LEP2 searches, and for the moment implement no other constraints, such as relic density, Higgs mass, *etc.*

2.1 Random scan results

Our first results are shown in Fig. 1, where we show points from the wide scan (dark blue) and points from the narrow scan (light blue) in the parameter versus R plane. From frame *a*), we see that Yukawa unification to better than 30% ($R < 1.3$) cannot be achieved for $m_{16} < 1 \text{ TeV}$, while Yukawa coupling unification becomes much more likely at multi-TeV values of m_{16} . Frame *b*) shows that Yukawa-unified models prefer $m_{10} \sim 1 - 1.3 m_{16}$, while frame *c*) shows that a positive value of $M_D^2 \sim (0.25 - 0.5) m_{16}^2$ which yields $m_{H_u}^2 < m_{H_d}^2$ is preferred. In frame *d*), we see that the best Yukawa-unified solutions are found for the lowest possible values of $m_{1/2}$. We note here that—using 1-loop RGEs along with the LEP2 constraint $m_{\tilde{\chi}_1^\pm} > 103.5 \text{ GeV}$ —one would expect from models with gaugino mass unification that since $m_{\tilde{\chi}_1^\pm} \sim M_2(\text{weak}) \sim 0.8 m_{1/2}$ that we would have $m_{1/2} \gtrsim 125 \text{ GeV}$ always. However, the very large values of m_{16} we probe alter the simple 1-loop gaugino mass unification condition (that $\frac{M_1}{\alpha_1} = \frac{M_2}{\alpha_2} = \frac{M_3}{\alpha_3}$) via 2-loop RGE effects. Thus, values of $m_{1/2}$ much lower than $\sim 125 \text{ GeV}$ are possible if m_{16} is large.

In frame *e*), we see a sharp dependence that Yukawa-unified solutions can only be obtained for $A_0 \sim -2m_{16}$, while frame *f*) shows that $\tan \beta$ must indeed be large: in the range $\sim 47 - 53$. Bagger *et al.* had shown in Ref. [14] that a radiatively-driven inverted scalar mass hierarchy with $m(\text{third generation}) \ll m(\text{first/second generation})$ could be derived provided one starts with unified Yukawa couplings, the boundary conditions

$$4m_{16}^2 = 2m_{10}^2 = A_0^2 \tag{2.2}$$

and one neglects the effect of gaugino masses. Our results in Fig. 1 show the *inverse* effect: that Yukawa coupling unification can only be achieved if one imposes the boundary conditions (2.2) along with $m_{16} \gg m_{1/2}$. This result holds only in our numerical calculations for

$\mu > 0$ and $A_0 < 0$ and of course $m_{H_u}^2 < m_{H_d}^2$. The results shown in Fig. 1 also verify that the results obtained in Ref. [18] still hold, even with updated spectra code and a lower value of $m_t = 171$ GeV.

In Fig. 2, we show various -ino masses³ versus R as generated from our random scan. In frame *a*), we see that—owing to the preference of Yukawa-unified solutions to have $m_{1/2}$ as small as possible, the chargino mass $m_{\tilde{\chi}_1^\pm}$ is preferred to be quite light, as close to the LEP2 limit as possible, with $m_{\tilde{\chi}_1^\pm} \sim 100$ – 200 GeV. Likewise, in frame *b*), the gluino mass should be relatively light, with $m_{\tilde{g}} \sim 350$ – 500 GeV. The lightest neutralino $\tilde{\chi}_1^0$ mass is shown in frame *c*), and is preferred in the range $m_{\tilde{\chi}_1^0} \sim 50$ – 100 GeV. Meanwhile, the mass difference $m_{\tilde{\chi}_2^0} - m_{\tilde{\chi}_1^0}$ is shown in frame *d*), and is also in the range ~ 50 – 100 GeV. This latter quantity is important because if $m_{\tilde{\chi}_2^0} - m_{\tilde{\chi}_1^0} < M_Z$, two body spoiler decay modes such as $\tilde{\chi}_2^0 \rightarrow \tilde{\chi}_1^0 Z$ will be kinematically closed, and the three body decays $\tilde{\chi}_2^0 \rightarrow \tilde{\chi}_1^0 \ell \bar{\ell}$ ($\ell = e$ or μ) should occur at a sufficiently large rate at the LHC that an edge should be visible in the $m(\ell \bar{\ell})$ invariant mass distribution at $m_{\tilde{\chi}_2^0} - m_{\tilde{\chi}_1^0}$ [30]. This measureable mass edge can serve as the starting point for sparticle mass reconstruction in SUSY particle cascade decay events at the LHC [31]. Thus, in Yukawa-unified models, this mass edge is highly likely to be visible.

In Fig. 3, we show the expected masses of *a*) \tilde{u}_L -squark, *b*) the \tilde{t}_1 -squark, *c*), the pseudoscalar Higgs boson A and *d*) the superpotential Higgs parameter μ . Frame *a*) shows that Yukawa-unified solutions prefer first/second generation squarks and sleptons with masses in the 5–20 TeV range—far higher than values typically examined in phenomenological SUSY studies! The top squark mass and the A , H and H^\pm Higgs bosons tends to be somewhat lighter: in the 2–8 TeV range. Finally, frame *d*) shows that the μ parameter—which is derived from the EWSB minimization conditions—tends also to be in the 5–15 TeV range. Thus, using a top-down approach to search for Yukawa-unified solutions in the HS model, we find that $\mu \gg M_1, M_2$, so that the lighter charginos and neutralinos should be gaugino-like, and quite light, while the heavier charginos and neutralino will be in the multi-TeV range, and nearly pure higgsino-like states. In particular, the lightest SUSY particle (LSP)—the neutralino $\tilde{\chi}_1^0$ —is nearly pure bino-like.

In Fig. 4, we plot R vs. $\Omega_{\tilde{\chi}_1^0} h^2$ for LEP2 allowed points from our random scan. It is clear that $R \sim 1$ points predict an extremely large value of $\Omega_{\tilde{\chi}_1^0} h^2$ of 30–30,000. On the other hand, if we require consistency with the WMAP-measured value of $\Omega_{\tilde{\chi}_1^0} h^2 \simeq 0.1$, then we generate Yukawa-unified solutions to 40% unification with the random scan. This plot underscores the difficulty of finding sparticle mass spectra solutions which are compatible with *both* the measured dark matter abundance and t – b – τ Yukawa coupling unification.

³We collectively refer to the set of all gluinos, charginos and neutralinos as -inos.

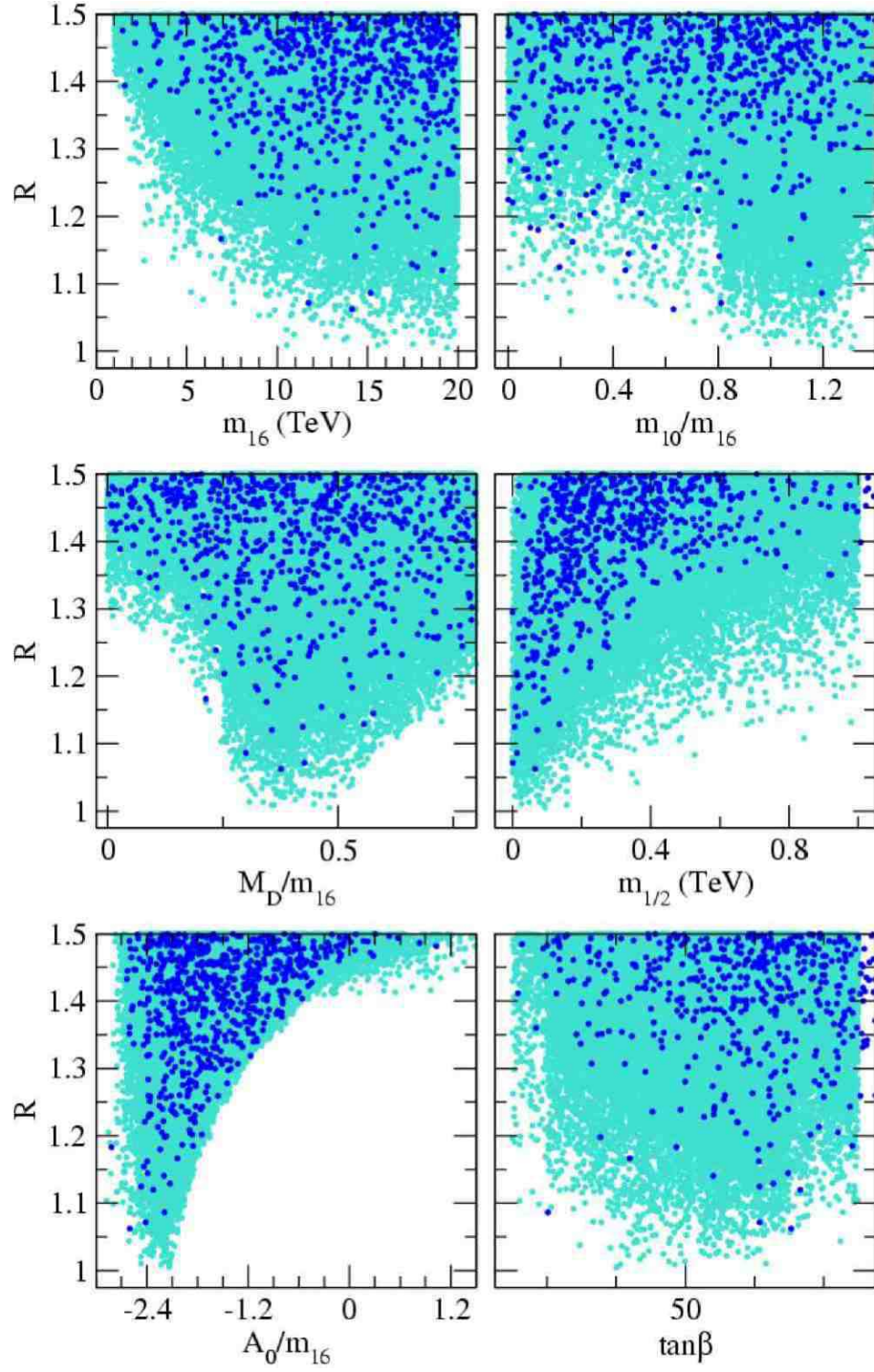


Figure 1: Plot of R versus various input parameters for a wide (dark blue) and narrow (light blue) random scan over the parameter ranges listed in Eq. (2.1). We take $\mu > 0$ and $m_t = 171$ GeV.

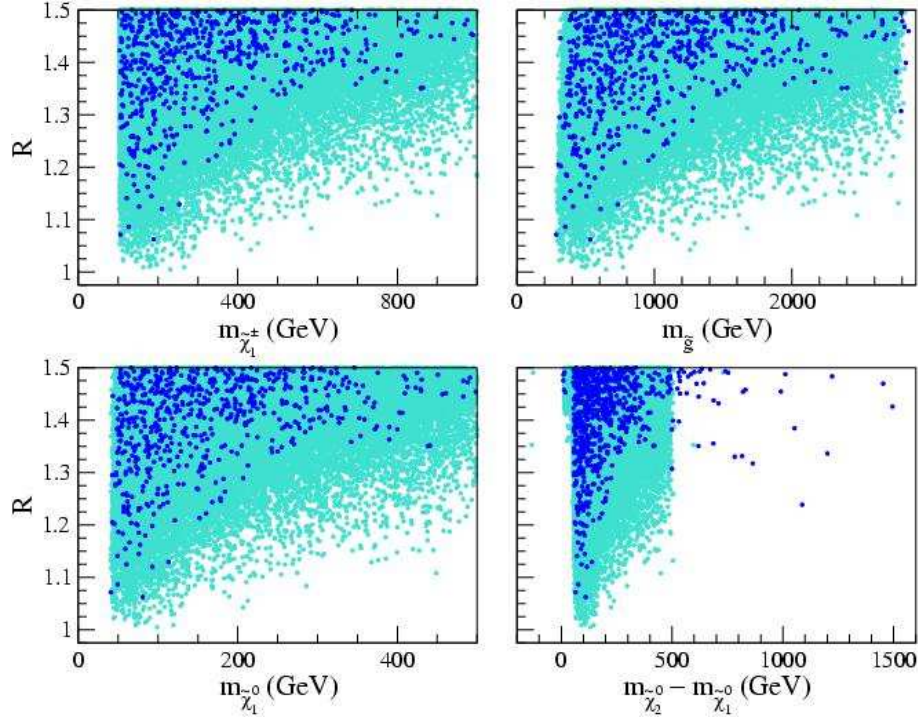


Figure 2: Plot of R versus various sparticle masses for a random scan over the parameter range listed in Eq. (2.1). We take $\mu > 0$ and $m_t = 171$ GeV.

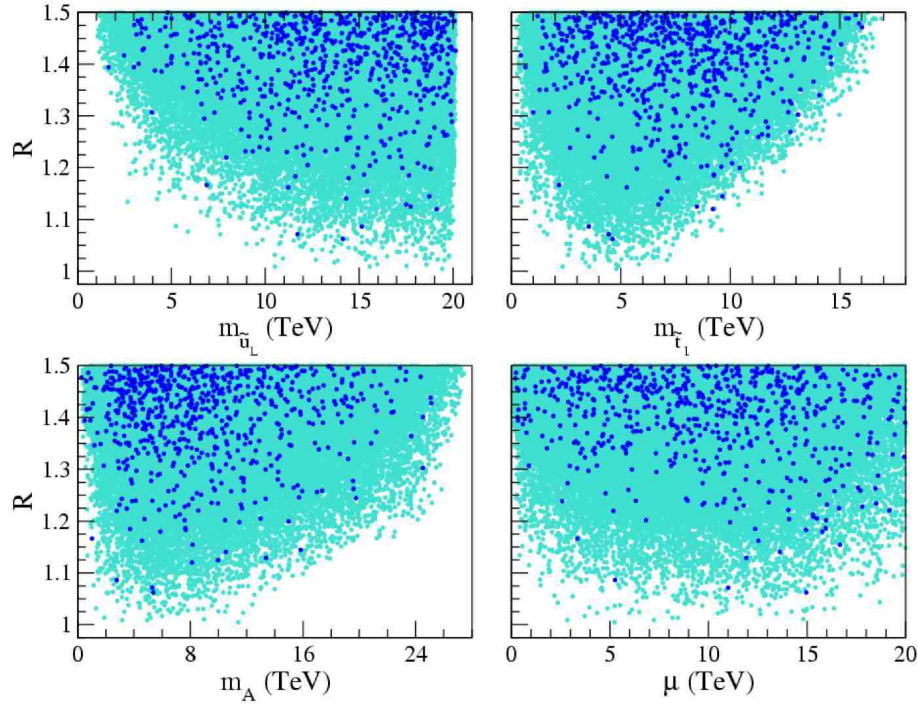


Figure 3: Plot of R versus various sparticle masses for a random scan over the parameter range listed in Eq. (2.1). We take $\mu > 0$ and $m_t = 171$ GeV.

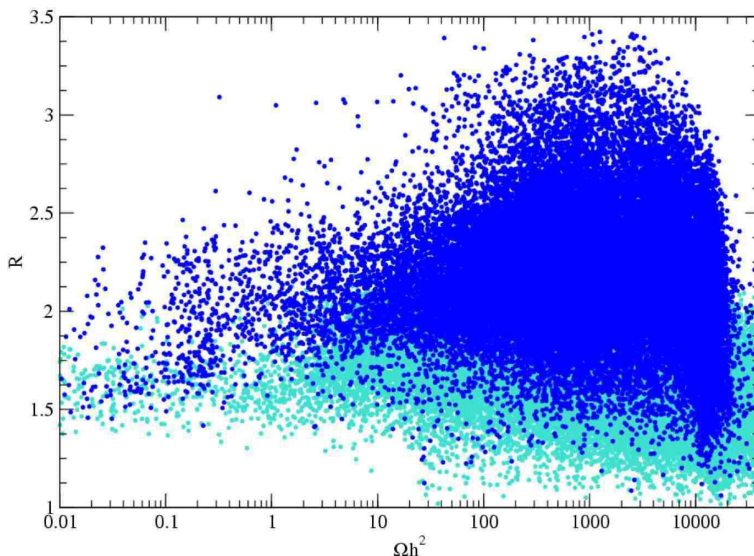


Figure 4: Plot of $\Omega_{\tilde{\chi}_1^0} h^2$ vs. R for a random scan over the parameter range listed in Eq. (2.1). We take $\mu > 0$ and $m_t = 171$ GeV.

2.2 Three proposals to reconcile Yukawa-unified models with dark matter relic density

2.2.1 Dark matter solution via neutralino decay to axino

We see from Fig. 4 that models generated from the random scan with $R \sim 1.0$ all have $\Omega_{\tilde{\chi}_1^0} h^2 \sim 30 - 30,000$: far beyond the WMAP-measured result of $\Omega_{CDM} h^2 \sim 0.1$. One possible solution to reconcile the predicted and measured dark matter density is to assume that the lightest neutralino $\tilde{\chi}_1^0$ is in fact not the LSP, but is unstable. Some alternative LSP candidates consist of the gravitino \tilde{G} or the axino \tilde{a} . In gravity-mediated SUSY breaking models, the gravitino mass $m_{3/2}$ arises due to the superHiggs mechanism, and is expected to set the scale for all the soft SUSY breaking terms. Usually it is assumed the gravitino is heavier than the lightest neutralino $m_{3/2} > m_{\tilde{\chi}_1^0}$, in which case the gravitino essentially decouples from phenomenology. However, if $m_{3/2} < m_{\tilde{\chi}_1^0}$, then the $\tilde{\chi}_1^0$ becomes unstable and can decay via modes such as $\tilde{\chi}_1^0 \rightarrow \gamma \tilde{G}$. The $\tilde{\chi}_1^0$ lifetime is expected to be very long— of order $10^4 - 10^{12}$ sec— so the neutralino still escapes detection at collider experiments, but is susceptible to constraints from Big Bang nucleosynthesis (BBN) and CMB anisotropies [32]. The relic density of gravitinos is expected to be simply $\Omega_{\tilde{G}} = \frac{m_{3/2}}{m_{\tilde{\chi}_1^0}} \Omega_{\tilde{\chi}_1^0} h^2$, since the gravitinos “inherit” the thermally produced neutralino relic number density. Thus, a scenario with a \tilde{G} superWIMP as LSP in SUGRA-type models can reduce the relic density by typically factors of a few— which is not enough in the case of Yukawa-unified models, where relic density suppression factors of $10^2 - 10^5$ are needed.

A better option occurs if we hypothesize an axino \tilde{a} LSP. If indeed there is a Peccei-Quinn solution to the strong CP problem, then one expects the existence of axions, typically with mass below the eV scale. While axions can themselves form cold dark matter, it is also easily possible that they contribute little to the CDM relic density. However, in

models with SUSY *and* axions, then the axion is just one element of an axion superfield, the superpartner of the axion being a spin- $\frac{1}{2}$ axino \tilde{a} . The axino mass can be far different from the typical soft SUSY breaking scale, and the range $m_{\tilde{a}} \sim \text{eV--GeV}$ is allowed.

Axinos can be produced in the early universe both thermally or non-thermally from NLSP decay. From the latter source, we expect roughly [33]

$$\Omega_{\tilde{a}} \sim \frac{m_{\tilde{a}}}{m_{\tilde{\chi}_1^0}} \Omega_{\tilde{\chi}_1^0} h^2. \quad (2.3)$$

Thus, for $\Omega_{\tilde{\chi}_1^0} \sim 10^3$ and with $m_{\tilde{\chi}_1^0} \sim 50 \text{ GeV}$ as in Yukawa-unified models, an axino mass of $m_{\tilde{a}} \lesssim 5 \text{ MeV}$ is required

In this mass range, the axinos from $\tilde{\chi}_1^0$ decay are expected to give a hot/warm component to the dark matter [34]. However, thermally produced axinos in this mass range could yield the required cold dark matter. Thus, if an unstable neutralino decay $\tilde{\chi}_1^0 \rightarrow \tilde{a}\gamma$ is to reconcile Yukawa-unified models with the relic density, then we would expect the dark matter to be predominantly cold axinos produced thermally, but with a re-heat temperature $T_R < T_f$, where T_f is the temperature where axinos decouple from the thermal plasma in the early universe. This scenario admits a dark matter abundance that can be in accord with WMAP measurements, and would be primarily CDM, but with a warm dark matter component arising non-thermally from $\tilde{\chi}_1^0$ decays. For a bino-like neutralino, as in Yukawa-unified models, the $\tilde{\chi}_1^0$ lifetime is given by [35]

$$\tau \simeq 3.3 \times 10^{-2} \text{sec} \frac{1}{C_{aYY}^2} \left(\frac{f_a/N}{10^{11} \text{GeV}} \right)^2 \left(\frac{50 \text{ GeV}}{m_{\tilde{\chi}_1^0}} \right)^3, \quad (2.4)$$

where the model-dependent constant C_{aYY} is of order 1, f_a is the Peccei-Quinn breaking scale, and N is a model dependent factor ($N = 1(6)$ for the KSVZ (DFSZ) axion model). Thus, for reasonable choices of model parameters, we expect the neutralino lifetime to be of order $3 \times 10^{-2} \text{ sec}$. This is short enough so that photon injection into the early universe from $\tilde{\chi}_1^0 \rightarrow \tilde{a}\gamma$ decay occurs *before* nucleosynthesis, thus avoiding constraints from BBN.

For illustration, we adopt a point A listed in Table 1 of Yukawa-unified benchmark models. The point has $m_{16} = 9202.9 \text{ GeV}$, $m_{10} = 10966.1 \text{ GeV}$, $M_D = 3504.4 \text{ GeV}$, $m_{1/2} = 62.5 \text{ GeV}$, $A_0 = -19964.5 \text{ GeV}$, $\tan \beta = 49.1$ GeV with $\mu > 0$ and $m_t = 171 \text{ GeV}$. It has $m_{\tilde{\chi}_1^0} = 55.6 \text{ GeV}$ and $\Omega_{\tilde{\chi}_1^0} h^2 = 423$ (IsaReD result). Thus, $\tilde{\chi}_1^0 \rightarrow \tilde{a}\gamma$ with $m_{\tilde{a}} \lesssim 1 \text{ MeV}$ would allow for a mixed warm/cold axino dark matter solution to the problem of relic density in Yukawa-unified models.

2.2.2 Dark matter solution via non-universal gaugino masses

An alternative solution to reconciling the dark matter abundance with Yukawa-unified models is to consider the possibility of non-universal gaugino masses. If we adopt any of the Yukawa unified models from the random scan and vary the $SU(2)$ ($SU(3)$) gaugino masses M_2 (M_3), then the Yukawa coupling unification will be destroyed via the effect of $\tilde{t}_i \tilde{\chi}_j^\pm$ ($\tilde{g}\tilde{q}$) loops. However, if M_1 is varied, Yukawa coupling unification is preserved since contributions to fermion masses from loops containing $\tilde{\chi}_1^0$ are small.

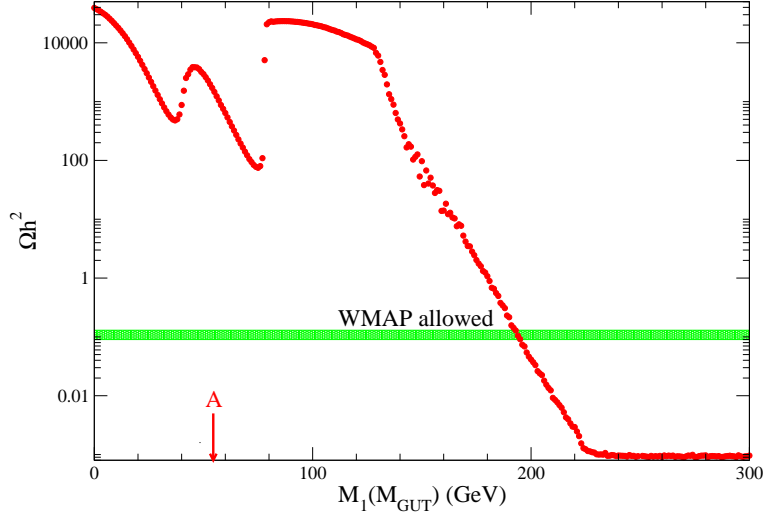


Figure 5: Plot of variation in $\Omega_{\tilde{\chi}_1^0} h^2$ versus non-universal GUT scale gaugino mass M_1 for benchmark point A in Table 1.

By raising the GUT scale value of M_1 to values higher than $m_{1/2}$, the weak scale value of M_1 is also increased. If M_1 is increased enough, then $m_{\tilde{\chi}_1^0}$ (which is nearly equal to M_1 since $\tilde{\chi}_1^0$ is largely bino-like) becomes close to $m_{\tilde{\chi}_1^\pm}$. When this happens, the $\tilde{\chi}_1^0$ becomes more wino-like, with an increased annihilation cross section to WW pairs if $m_{\tilde{\chi}_1^0} > M_W$ [36]. In our case, usually $m_{\tilde{\chi}_1^0} < M_W$. Then raising M_1 still lowers the relic density, but now via bino-wino co-annihilation (BWCA) [24].

In Fig. 5 we show the variation in $\Omega_{\tilde{\chi}_1^0} h^2$ versus $M_1(M_{GUT})$ for benchmark point A in Table 1. The location of M_1 for point A is marked by the arrow. The double dips at low M_1 are due to neutralino annihilation through the Z and h poles. Once $M_1(M_{GUT})$ is increased to ~ 195 GeV, then we reach a relic density in accord with WMAP measurements. Since $m_{\tilde{\chi}_1^\pm} \simeq m_{\tilde{\chi}_1^0}$, and $m_{\tilde{\chi}_1^\pm} \sim m_{\tilde{\chi}_1^0}$, the $\tilde{\chi}_2^0 - \tilde{\chi}_1^0$ mass gap is small, of order 10–20 GeV. We list the raised $M_1(M_{GUT}) = 195$ GeV point as point B in benchmark Table 1.

2.2.3 Dark matter solution via generational non-universality

Another possibility for reconciling the neutralino relic density with the measured value is to lower the first/second generation scalar masses $m_{16}(1,2)$, while keeping $m_{16}(3)$ fixed at m_{16} . The Bagger *et al.* inverted hierarchy solution depends only on third generation scalar masses, while the effects of the first two generations decouple. Ordinarily, solutions with $m_{16}(1,2) = m_{16}(3)$ are taken to enforce the super-GIM mechanism for suppression of flavor changing neutral current (FCNC) processes. Limits from FCNCs mainly require near degeneracy between the first two generations, while limits on third generation universality are much less severe [37]. Lowering $m_{16}(1,2)$ works to lower the relic density because of the large S term in the scalar mass RGEs:

$$S = m_{H_u}^2 - m_{H_d}^2 + \text{Tr} [\mathbf{m}_Q^2 - \mathbf{m}_L^2 - 2\mathbf{m}_U^2 + \mathbf{m}_D^2 + \mathbf{m}_E^2]. \quad (2.5)$$

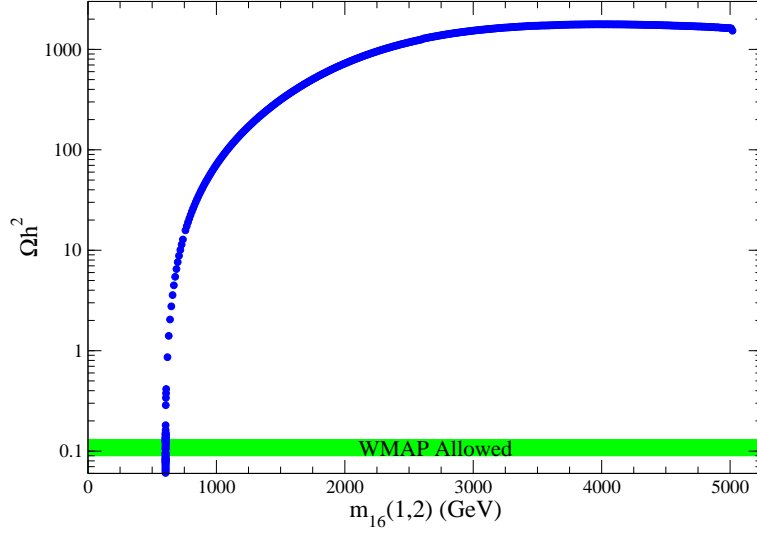


Figure 6: Plot of variation in $\Omega_{\tilde{\chi}_1^0} h^2$ versus non-universal GUT scale first/second generation scalar mass $m_{16}(1,2)$ for benchmark point C in Table 1.

In models with universality, like mSUGRA, $S = 0$ to one-loop at all energy scales; in models with non-universal Higgs scalars, like the HS model, this term can be large and have a major influence on scalar mass running. The large S term helps suppress right-squark masses. If $m_{16}(1,2)$ is taken light enough, then $m_{\tilde{u}_R} \simeq m_{\tilde{c}_R} \simeq m_{\tilde{\chi}_1^0}$, and neutralino-pair annihilation into quarks and neutralino-squark co-annihilation can act to reduce the relic density.

In Fig. 6, we show the variation in $\Omega_{\tilde{\chi}_1^0} h^2$ versus $m_{16}(1,2)$ where we take $m_{16}(3) = 5018.8$ GeV, $m_{1/2} = 160$ GeV, $A_0 = -10624.2$ GeV, $\tan \beta = 47.8$ and $\mu > 0$. When $m_{16}(1,2)$ is lowered to 603.8 GeV, then $m_{\tilde{u}_R} \simeq m_{\tilde{c}_R} = 98.3$ GeV, and we have neutralino annihilation via light t -channel squark exchange and also neutralino-squark co-annihilation.⁴ IsaReD and Micromegas give $\Omega_{\tilde{\chi}_1^0} h^2 \sim 0.1$ at this point, which we adopt as benchmark point C in Table 1. The two light squarks are just at the limit of LEP2 exclusion. They may possibly be excludable by Tevatron analyses, but the squark-neutralino mass gap is quite small, so the energy release from $\tilde{u}_R \rightarrow u \tilde{\chi}_1^0$ is low. So far, no such study has been made, and so the possibility cannot yet be definitively excluded.

⁴A bug fix is needed in the Isajet 7.75 IsaReD subroutine in order to obtain the correct relic density; we thank A. Pukhov for pointing this out.

3. Markov Chain Monte Carlo analysis

Next we adopt an improved scanning method based on the Markov Chain Monte Carlo (MCMC) technique to search more efficiently for parameter space regions of good Yukawa unification and WMAP-compatible DM relic density. A Markov Chain [38] is a discrete-time, random process having the Markov property, which is defined such that given the present state, the future state only depends on the present state, but not on the past states. That is:

$$P(X^{t+1} = x | X^t = x^t, \dots, X^1 = x^1) = P(X^{t+1} = x | X^t = x^t). \quad (3.1)$$

An MCMC constructs a Markov Chain through sampling from a parameter space with the help of a specified algorithm. In this study, we have applied the Metropolis-Hastings algorithm [39], which generates a candidate state x^c from the present state x^t using a proposal density $Q(x^t; x^c)$. The candidate state is accepted to be the next state x^{t+1} if the ratio

$$p = \frac{P(x^c)Q(x^t; x^c)}{P(x^t)Q(x^c; x^t)}, \quad (3.2)$$

(where $P(x)$ is the probability calculated for the state x) is greater than a uniform random number $a = U(0, 1)$. If the candidate is not accepted, the present state x^t is retained and a new candidate state is generated. For the proposal density we use a Gaussian distribution that is centered at x^t and has a width σ . This simplifies the p ratio to $P(x^c)/P(x^t)$.

Once taking off from a starting point, Markov chains are aimed to converge at a target distribution $P(x)$ around a point with the highest probability. The time needed for a Markov chain to converge depends on the width of the Gaussian distribution used as the proposal density. This width can be adjusted during the run to achieve a more efficient convergence.

In our search in the $SO(10)$ parameter space, we assume flat priors and we approximate the likelihood of a state to be $e^{-\chi^2(x)}$. We define the χ^2 for R as

$$\chi_R^2 = \left(\frac{R(x) - R_{unification}}{\sigma_R} \right)^2 \quad (3.3)$$

where $R_{unification} = 1$ and σ_R is the discrepancy we allow from absolute Yukawa unification, which, in this case we take to be 0.05. On the other hand, for Ωh^2 we define

$$\chi_{\Omega h^2}^2 = \begin{cases} 1, & (0.094 \leq \Omega h^2 \leq 0.136) \\ \left(\frac{\Omega h^2(x) - \Omega h_{mean}^2}{\sigma_{\Omega h^2}} \right)^2, & (\Omega h^2 < 0.094 \text{ or } \Omega h^2 > 0.136) \end{cases} \quad (3.4)$$

where $\Omega h_{mean}^2 = 0.115$ is the mean value of the range $0.094 < \Omega h^2 < 0.136$ proposed in [40], and $\sigma_{\Omega h^2} = 0.021$. This way, the MCMC primarily searches for regions of Yukawa unifications, and within these regions for solutions with a good relic density.

For each search, we select a set of ~ 10 starting points in order to ensure a more thorough investigation of the parameter space. Then we run the MCMC, aiming to maximize

the likelihood of either R alone, or R and Ωh^2 simultaneously. For the case of simultaneous maximization, we compute the p ratios for R and Ωh^2 individually, requiring both $p_R > a$ and $p_{\Omega h^2} > a$ separately. We do not strictly seek convergence to an absolute maximal likelihood, but we rather use the MCMC as a tool to reach compatible regions and to investigate the amount of their extension in the $SO(10)$ parameter space.

3.1 HS model: neutralino annihilation via h resonance

We begin our MCMC scans by selecting 10 starting points “pseudorandomly” –that is, selecting them from different m_{16} regions to cover a wider range of the parameter space– and imposing some loose limits (defined by our previous works and random scans) on the rest of their parameters to achieve a more efficient convergence. Our initial scan is directed to look for points only with R as close to 1.0 as possible by maximizing solely the likelihood of R . Based on the results of the first MCMC scan, we then pick a new set of 10 starting points with low R and also low $\Omega_{\tilde{\chi}_1^0} h^2$, and direct the second scan to look for points with both $R = 1.0$ and $\Omega_{\tilde{\chi}_1^0} h^2 < 0.136$ by maximizing the likelihoods of R and Ωh^2 simultaneously. For MCMC scans, the code is interfaced to the micrOMEGAs [41] package to evaluate the relic density and low-energy constraints.

Figure 7 shows the Yukawa-unified region found by the MCMC results as a projection in the plane of m_{16} versus m_{10} . The light-blue dots are points which have $R < 1.1$, while dark blue dots have $R < 1.05$. In addition, we show in orange (red) the points which satisfy $R < 1.1$ (1.05) and $\Omega_{\tilde{\chi}_1^0} h^2 < 0.136$. The points with low R are narrowly correlated along the line $m_{10} \simeq 1.2m_{16}$. While the low R points range over m_{16} values from 3 to over 12 TeV (in agreement with the results from the random scans) the MCMC has also identified a range of points with *both* $R \simeq 1$ and $\Omega_{\tilde{\chi}_1^0} h^2 < 0.136$, but only for m_{16} values of about 3–4 TeV!

Fig. 8 shows the MCMC scan results in the m_{16} vs. A_0/m_{16} plane. Again, we see that points with low R populate the region with $A_0 \sim (2\text{--}2.1)m_{16}$ over a wide range of m_{16} values. The plot includes the $\Omega_{\tilde{\chi}_1^0} h^2 < 0.136$ points around $m_{16} \sim 3\text{--}4$ TeV.

In Fig. 9, we show MCMC results in the m_{16} vs. $m_{1/2}$ plane. Here, we see the very lowest R points select out the lowest possible $m_{1/2}$ values allowed for a given value of m_{16} , and that the minimum $m_{1/2}$ value allowed steadily decreases with increasing m_{16} –the boundary being determined by the LEP2 limit on chargino masses. The points with a “good” relic density are clustered around $m_{1/2} \sim 100$ GeV.

We also show in Fig. 10 the individual GUT-scale values of Higgs soft terms m_{H_u} (lower branch) and m_{H_d} (upper branch). This plot displays the required Higgs splitting and confirms that $m_{H_d} > m_{H_u}$.

In Fig. 11, we show points with low R in the $m_h - 2m_{\tilde{\chi}_1^0}$ vs. $m_A - 2m_{\tilde{\chi}_1^0}$ plane. In these solutions, m_A is usually far greater than $2m_{\tilde{\chi}_1^0}$, indicating the neutralino annihilation through the A -resonance is not the cause of the reduced relic density orange and red points. However, the low $\Omega_{\tilde{\chi}_1^0} h^2$ points all *do* lie along the $m_h \simeq 2m_{\tilde{\chi}_1^0}$ line, indicating that h -resonance annihilation is the mechanism at work to reduce the relic density in the early universe. In Fig. 12, we show R vs. $\Omega_{\tilde{\chi}_1^0} h^2$ for the MCMC scan. In this frame, we see that

the points with high relic density extend down to $R = 1$, while the low relic density points reach below $R = 1.05$, but can reach no lower than $R = 1.03$.

We are now in a position to understand this new class of Yukawa-unified, DM-allowed solutions: the search for low R pushes m_{16} to very high, multi-TeV values. Meanwhile, in order for h -resonance annihilation to reduce the relic density to the WMAP-allowed range, m_{16} can't be too large. The region around $m_{16} \sim 3\text{--}4$ TeV offers a compromise between these two tendencies: for m_{16} not too large, the dip in relic density due to the h -resonance annihilation is sufficient to bring the relic density into the desired range. But since m_{16} can't be too large, the Yukawa unification is limited to a couple of percent at best. This new class of solutions was difficult to reach using a random scan, since the h -resonance is so narrow. The necessary value of $m_{\tilde{\chi}_1^0}$ has to be just right— with $2m_{\tilde{\chi}_1^0}$ slightly below m_h — so that the thermal averaging of neutralino energies convolutes with the resonant cross section with enough strength to give substantial neutralino annihilation in the early universe.

The $SO(10)$ model parameters leading to low R and good relic density occur only over a very narrow range of $m_{1/2} \sim 100$ GeV and $m_{16} \sim 3$ TeV. This means the Yukawa-unified h -resonance annihilation points have very specific mass spectra predictions. We show in Fig. 13 the $m_{\tilde{g}}$ vs. $m_{\tilde{t}_1}$ plane for MCMC points in the HS model. Here, we see that the points with $\Omega_{\tilde{\chi}_1^0} h^2 < 0.136$ all have $m_{\tilde{g}} \sim 350\text{--}450$ GeV, while $m_{\tilde{t}_1} \sim 350\text{--}750$ GeV. The large μ parameter combines with gaugino mass unification to predict that $m_{\tilde{\chi}_1^\pm} \simeq m_{\tilde{\chi}_2^0} \sim 100\text{--}150$ GeV, while $m_{\tilde{\chi}_1^0} \sim 50\text{--}75$ GeV.

Given this very tightly correlated mass spectrum, gluino cascade decay events at the LHC will lead to $\tilde{\chi}_2^0$ production, followed mainly by $\tilde{\chi}_2^0 \rightarrow \tilde{\chi}_1^0 b \bar{b}$ decay and also by $\tilde{\chi}_2^0 \rightarrow \tilde{\chi}_1^0 \ell \bar{\ell}$ decay. The OS/SF isolated dilepton mass spectrum will be bounded kinematically by $m_{\tilde{\chi}_2^0} - m_{\tilde{\chi}_1^0}$. The mass difference provides an edge in the dilepton mass spectrum which is characteristic of these decays, and which is easily measureable. Furthermore, it should be correlated with m_h , since all these masses are related by resonance annihilation and theory. The value of m_h should be directly measureable at LHC after several years of data taking via the bump in the $h \rightarrow \gamma\gamma$ mass spectrum. Thus, we plot in Fig. 14 our Yukawa-unified MCMC points in the $m_{\tilde{\chi}_2^0} - m_{\tilde{\chi}_1^0}$ vs. m_h plane. For this scenario to be borne out, we would predict $m_{\tilde{\chi}_2^0} - m_{\tilde{\chi}_1^0} \sim 52\text{--}65$ GeV, with a roughly linear correlation with m_h .

We adopt point D in Table 1 as being representative of the light Higgs h -resonance annihilation compromise solutions. The relic density computed with micrOMEGAs ($\Omega_{\tilde{\chi}_1^0} h^2 = 0.06$) is below the preferred range, while IsaReD gives $\Omega_{\tilde{\chi}_1^0} h^2 = 0.1$. Yukawa couplings are unified at the 9% level. We note here that we could have adopted a solution with even better Yukawa coupling unification at the 4–5% level. These solutions tend to give light Higgs mass $m_h \lesssim 110$ GeV (as can be seen by the red dots in Fig. 14) which are more likely to be excluded by LEP2 Higgs search results.

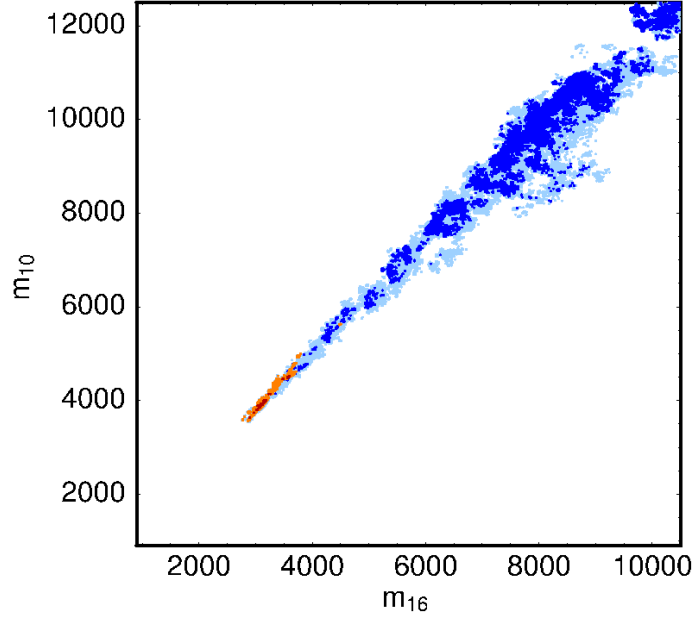


Figure 7: Plot of MCMC results in the m_{16} vs. m_{10} plane; the light-blue (dark-blue) points have $R < 1.1$ (1.05), while for the orange (red) points $R < 1.1$ (1.05) and $\Omega_{\tilde{\chi}_1^0} h^2 < 0.136$.

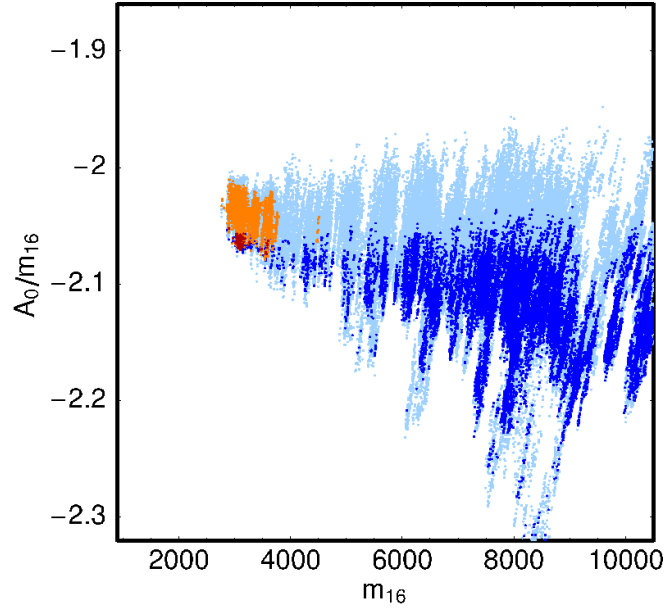


Figure 8: Plot of MCMC results in the m_{16} vs. A_0/m_{16} plane; the light-blue (dark-blue) points have $R < 1.1$ (1.05), while for the orange (red) points $R < 1.1$ (1.05) and $\Omega_{\tilde{\chi}_1^0} h^2 < 0.136$.

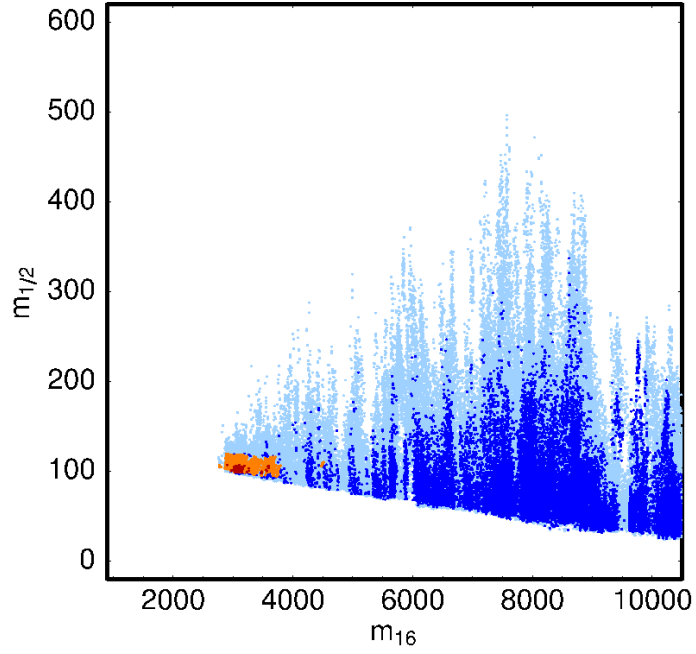


Figure 9: Plot of MCMC results in the m_{16} vs. $m_{1/2}$ plane; the light-blue (dark-blue) points have $R < 1.1$ (1.05), while for the orange (red) points $R < 1.1$ (1.05) and $\Omega_{\tilde{\chi}_1^0} h^2 < 0.136$.

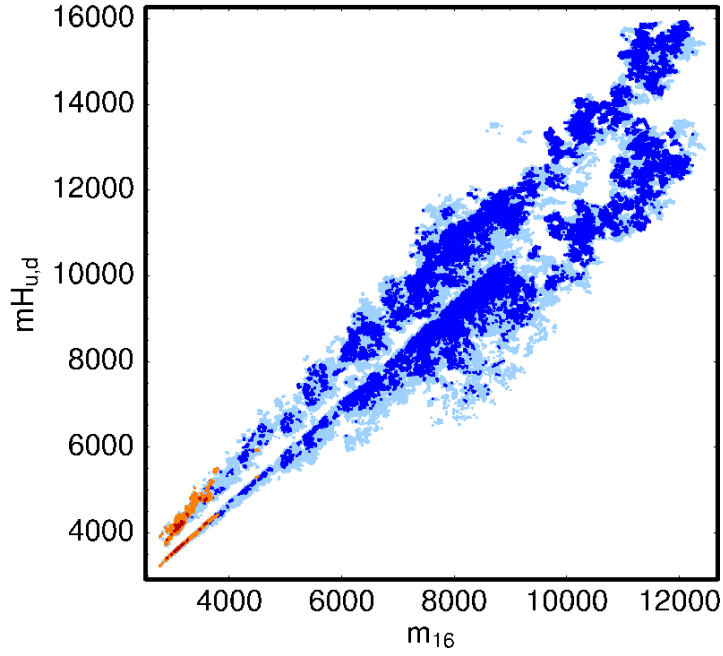


Figure 10: Plot of MCMC results in the m_{16} vs. $m_{H_{d,u}}$ plane; the light-blue (dark-blue) points have $R < 1.1$ (1.05), while for the orange (red) points $R < 1.1$ (1.05) and $\Omega_{\tilde{\chi}_1^0} h^2 < 0.136$.

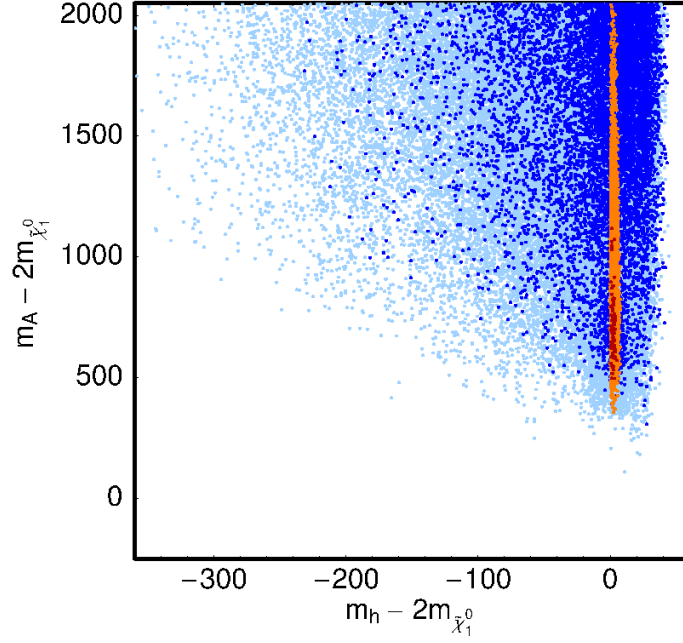


Figure 11: Plot of MCMC results in the $m_h - 2m_{\tilde{\chi}_1^0}$ vs. $m_A - 2m_{\tilde{\chi}_1^0}$ plane; the light-blue (dark-blue) points have $R < 1.1$ (1.05), while for the orange (red) points $R < 1.1$ (1.05) and $\Omega_{\tilde{\chi}_1^0} h^2 < 0.136$.

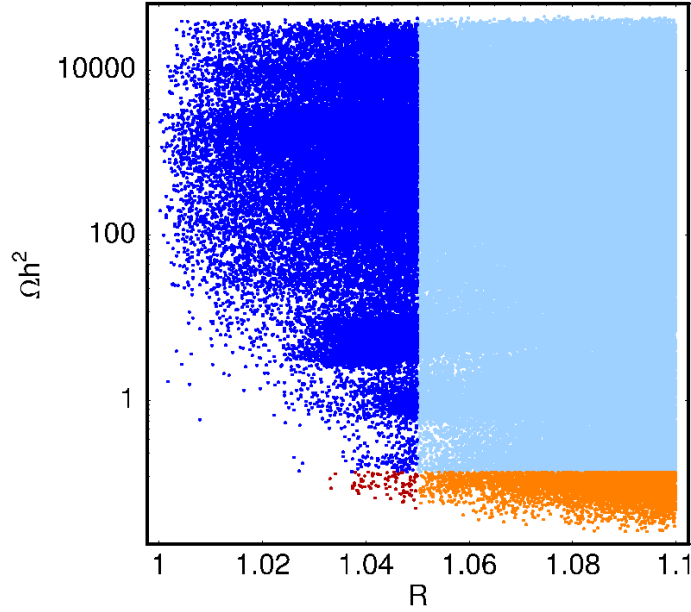


Figure 12: Plot of MCMC results in the R vs. $\Omega_{\tilde{\chi}_1^0} h^2$ plane; the light-blue (dark-blue) points have $R < 1.1$ (1.05), while for the orange (red) points $R < 1.1$ (1.05) and $\Omega_{\tilde{\chi}_1^0} h^2 < 0.136$.

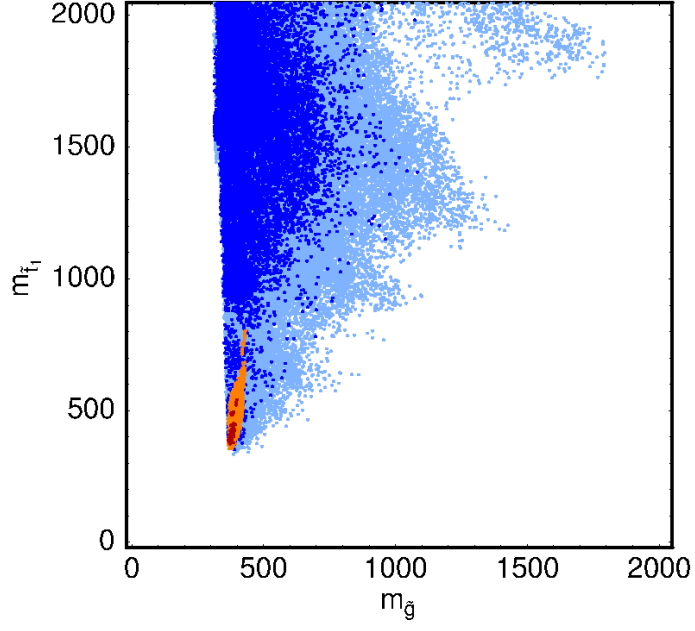


Figure 13: Plot of MCMC results in the $m_{\tilde{g}}$ vs. $m_{\tilde{t}_1}$ plane; the light-blue (dark-blue) points have $R < 1.1$ (1.05), while for the orange (red) points $R < 1.1$ (1.05) and $\Omega_{\tilde{\chi}_1^0} h^2 < 0.136$.

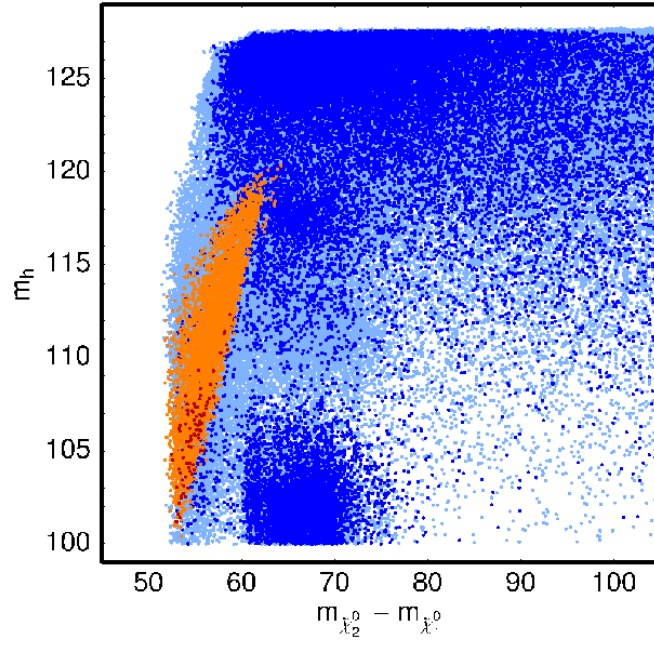


Figure 14: Plot of MCMC results in the $m_{\tilde{\chi}_2^0} - m_{\tilde{\chi}_1^0}$ vs. m_h plane; the light-blue (dark-blue) points have $R < 1.1$ (1.05), while for the orange (red) points $R < 1.1$ (1.05) and $\Omega_{\tilde{\chi}_1^0} h^2 < 0.136$.

3.2 Solutions using weak scale Higgs boundary conditions

In the analysis put forth by BDR [4], Yukawa-unified solutions are found with low values of both μ and m_A in the 100–200 GeV range, while m_{16} and m_{10} are typically at the 2–3 TeV scale. We have seen from our results so far that μ and m_A are typically in the TeV regime. Some low μ solutions were generated using Isajet in Table 2 of Ref. [18], but these had $R \sim 1.25$.

We find here that we can generate small μ and small m_A solutions using Isajet by using the pre-programmed non-universal Higgs model (NUHM)⁵. The approach is to start with a set of GSH soft term boundary conditions, and evolve the soft SUSY breaking Higgs masses $m_{H_u}^2$ and $m_{H_d}^2$ down to the weak scale M_{SUSY} . At $Q = M_{SUSY}$, re-calculate what $m_{H_u}^2$ and $m_{H_d}^2$ *should have been* in order to get the input values of m_A and μ , using the two electroweak symmetry breaking minimization conditions (in practise, we use 1-loop relations):

$$B = \frac{(m_{H_u}^2 + m_{H_d}^2 + 2\mu^2) \sin 2\beta}{2\mu} \quad \text{and} \quad (3.5)$$

$$\mu^2 = \frac{m_{H_d}^2 - m_{H_u}^2 \tan^2 \beta}{(\tan^2 \beta - 1)} - \frac{M_Z^2}{2}. \quad (3.6)$$

Then run back up to the GUT scale using these new WSH boundary conditions. At each iteration, the weak scale values of $m_{H_u}^2$ and $m_{H_d}^2$ have to be re-computed so as to maintain the input value of μ and m_A ; in this case, the GUT scale values of $m_{H_u}^2$ and $m_{H_d}^2$ are outputs, instead of inputs. For this class of solutions, both GSH *and* WSH boundary conditions must be used in Isajet. The GSH boundary conditions are needed just to get an acceptable EWSB on the first iteration so that a spectrum can be computed, and then modified to yield the input values of m_A and μ . Using default universal GSH soft terms will usually fail to give appropriate EWSB on any iteration where Yukawa couplings are unified.

We implement an MCMC scan over the modified parameter space

$$m_{16}, m_{1/2}, A_0, \tan \beta, m_A, \mu \quad (3.7)$$

(effectively trading the GUT scale inputs $m_{H_u}^2$ and $m_{H_d}^2$ (or alternatively m_{10} and M_D^2) for weak scale inputs m_A and μ). We begin with 10 starting points selected pseudorandomly from different regions of the above parameter space, and implement two MCMC scans on them, one searching for points with lowest R values by maximizing the likelihood of R and the other for solutions with $R = 1$ and $\Omega_{\tilde{\chi}_1^0} h^2 < 0.136$ by maximizing likelihoods of R and Ωh^2 simultaneously.

Our first results are shown in Fig. 15 for the m_{16} vs. A_0/m_{16} plane, where we plot points with $R < 1.1$ (1.05) using dark blue (light blue) dots, and solutions with $\Omega_{\tilde{\chi}_1^0} h^2 < 0.136$ for $R < 1.1$ (1.05) using orange (red) dots. While we again get good Yukawa-unified solutions over a wide range of multi-TeV values of m_{16} , this time we pick up *additional* dark matter allowed solutions for $m_{16} : 3\text{--}6$ TeV. The solutions again respect the Bagger *et al.* boundary condition $A_0 \simeq -2m_{16}$.

⁵This is model line 8 of the Isajet non-universal supergravity models (NUSUG)

In Fig. 16, we show the WSH solutions in the m_{16} vs. $m_{1/2}$ plane. The minimum in allowed $m_{1/2}$ values again decreases with increasing m_{16} . We see that for the WSH class of solutions, much larger values of $m_{1/2}$ ranging up to 300 – 500 GeV are DM-allowed.

In Fig. 17, we plot the WSH solutions in the input parameter m_A vs. μ plane. In this case, we see that the bulk of the DM-allowed solutions occur at relatively low values of $m_A \sim 130$ –250 GeV. These low m_A solutions were extremely difficult to generate with the top-down approach, and indicate that they have a high degree of fine-tuning.⁶ A scattering of DM-allowed dots occur with high m_A values. These turn out to be the h -resonance solutions as generated with the GSH boundary conditions in Sec. 3.1.

This is seen more clearly by plotting in the $m_h - 2m_{\tilde{\chi}_1^0}$ vs. $m_A - 2m_{\tilde{\chi}_1^0}$ plane in Fig. 18. Here we see a narrow strip at $m_h - 2m_{\tilde{\chi}_1^0} = 0$ corresponding to h -resonance annihilation solutions, while we also have a wider band of solutions at $m_A - 2m_{\tilde{\chi}_1^0} = 0$, which indicate neutralino annihilation through the A -resonance. The width of the latter band is due to the fact that the A width can be quite wide— typically a few GeV, while the h -width is much narrower, of order 50 MeV.

The A -resonance solutions occur at $\tan \beta \sim 50$ and relatively low m_A values. This can signal dangerously high branching fractions for $B_s \rightarrow \mu^+ \mu^-$ decay [42] since the branching fraction goes like $\tan^6 \beta / m_A^4$. We plot the $BF(B_s \rightarrow \mu^+ \mu^-)$ vs. m_h in Fig. 19. The recent experimental limit from the CDF collaboration is that $BF(B_s \rightarrow \mu^+ \mu^-) < 5.8 \times 10^{-8}$ [43]. Thus, the entire band of A -resonance annihilation solutions becomes excluded! The smattering of DM-allowed dots below the CDF limit all occur with DM annihilation via the h -resonance.

In case these A -resonance solutions are somehow allowed— say by additional flavor-violating soft terms— we plot the solutions in the $m_{\tilde{g}}$ vs. $m_{\tilde{\chi}_1^0}$ plane in Fig. 20. Here, we see a much larger range of $m_{\tilde{g}}$ and $m_{\tilde{\chi}_1^0}$ values are DM-allowed than in the GSH solutions, with $m_{\tilde{g}}$ extending up to 1500 GeV.

If the DM-allowed GSH solutions are able to avoid the $BF(B_s \rightarrow \mu^+ \mu^-)$ constraint, then the values of m_A and $m_{\tilde{\chi}_2^0} - m_{\tilde{\chi}_1^0}$ will be correlated, and the latter quantity will be measureable if the mass gap $m_{\tilde{\chi}_2^0} - m_{\tilde{\chi}_1^0} < M_Z$. The predicted correlation is shown in Fig. 21. In this case, the mass gap $m_{\tilde{\chi}_2^0} - m_{\tilde{\chi}_1^0}$ runs far beyond M_Z .

We present a benchmark point with low m_A and $R \simeq 1$ as point E in Table 1. While the point is DM-allowed, it also violates the CDF bound on $BF(B_S \rightarrow \mu^+ \mu^-)$.

At this point, it is useful to compare the Isajet SUSY spectral solutions to those generated by Dermisek *et al.* in Ref. [20] and [21]. In Fig. 22, we plot the Isajet 7.75 solutions in the $m_{1/2}$ vs. μ plane for $m_{16} = 3$ TeV, $m_{10}/m_{16} = 1.3$, $A_0/m_{16} = -1.85$, $\tan \beta = 50.9$ and $\Delta m_H^2 = 0.14$, with $m_A = 500$ GeV: *i.e.* corresponding closely to Fig. 1 of [20]. We plot contours of R from 1.15 to 1.3. Also, the green-shaded regions give the WMAP-measured relic density, while white-shaded regions give $\Omega_{\tilde{\chi}_1^0} h^2 < 0.095$, and pink-shaded regions give $\Omega_{\tilde{\chi}_1^0} h^2 > 0.13$ (as in Dermisek *et al.*). The LEP2 constraint on $m_{\tilde{\chi}_1^\pm}$ is indicated by the solid contour at low $m_{1/2}$ and low μ . We see qualitatively the same

⁶The TW paper (Ref. [16]) remarks that there must be considerable fine-tuning as well to reconcile $BF(b \rightarrow s\gamma)$ with Yukawa unification and the dark matter relic abundance.

shape to the DM-allowed regions as generated by Dermisek *et al.*: the thick green regions are DM-allowed either by A -resonance annihilation at large μ , or by mixed higgsino DM

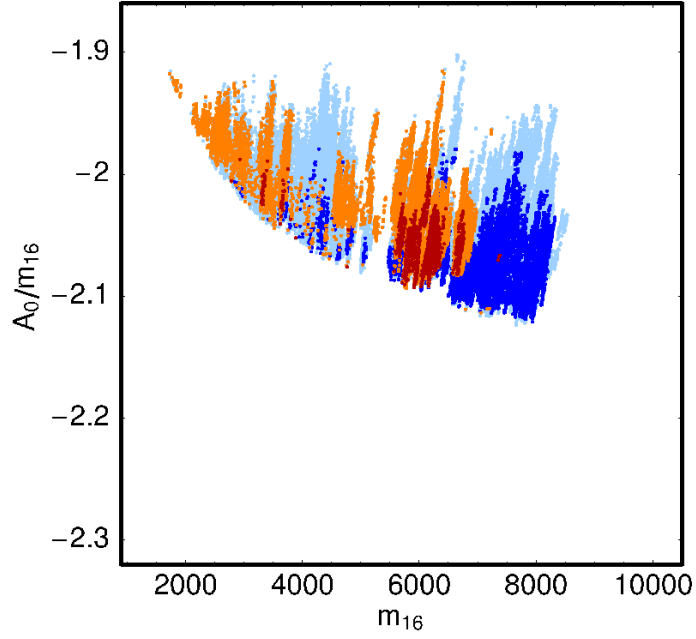


Figure 15: Plot of MCMC results using WSH boundary conditions in the m_{16} vs. A_0/m_{16} plane; the light-blue (dark-blue) points have $R < 1.1$ (1.05), while for the orange (red) points $R < 1.1$ (1.05) and $\Omega_{\tilde{\chi}_1^0} h^2 < 0.136$.

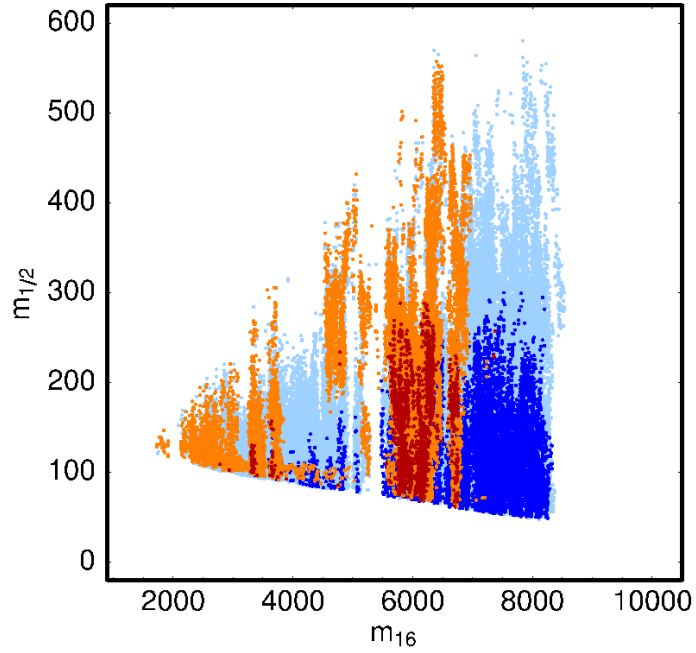


Figure 16: Plot of MCMC results using WSH boundary conditions in the m_{16} vs. $m_{1/2}$ plane; the light-blue (dark-blue) points have $R < 1.1$ (1.05), while for the orange (red) points $R < 1.1$ (1.05) and $\Omega_{\tilde{\chi}_1^0} h^2 < 0.136$.

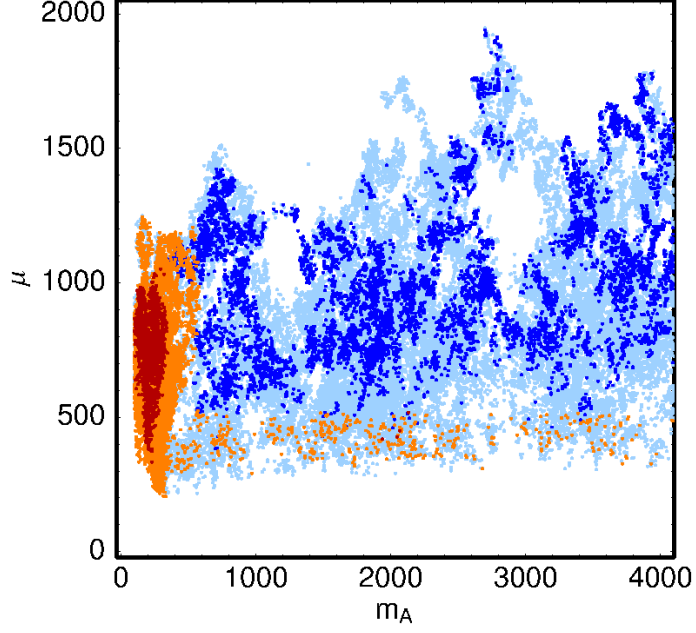


Figure 17: Plot of MCMC results using WSH boundary conditions in the m_A vs. μ plane; the light-blue (dark-blue) points have $R < 1.1$ (1.05), while for the orange (red) points $R < 1.1$ (1.05) and $\Omega_{\tilde{\chi}_1^0} h^2 < 0.136$.

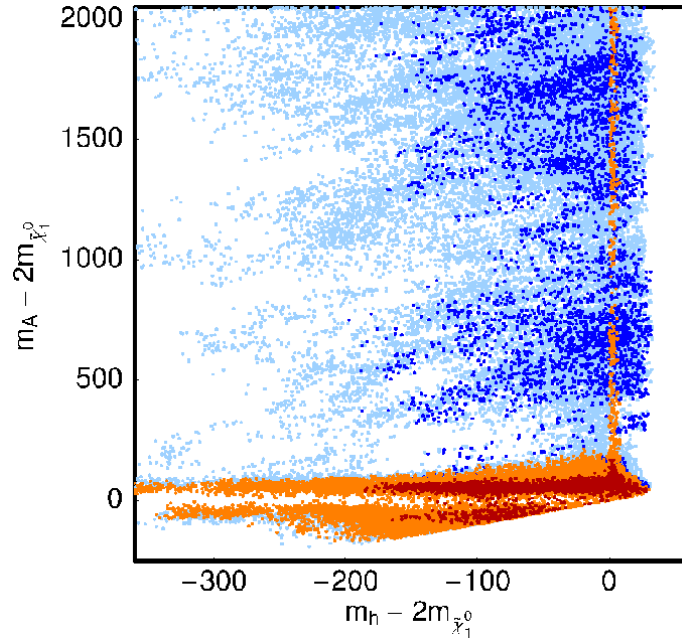


Figure 18: Plot of MCMC results using WSH boundary conditions in the $m_h - 2m_{\tilde{\chi}_1^0}$ vs. $m_A - 2m_{\tilde{\chi}_1^0}$ plane; the light-blue (dark-blue) points have $R < 1.1$ (1.05), while for the orange (red) points $R < 1.1$ (1.05) and $\Omega_{\tilde{\chi}_1^0} h^2 < 0.136$.

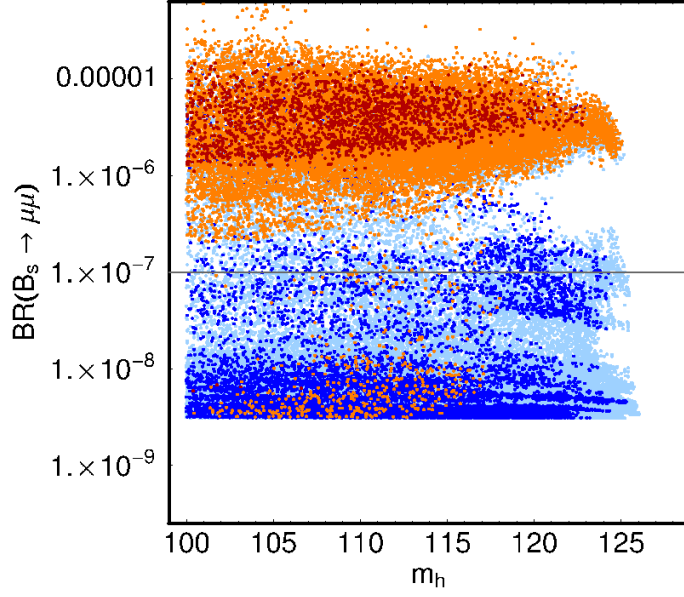


Figure 19: Plot of MCMC results using WSH boundary conditions in the m_h vs. $BF(B_s \rightarrow \mu^+ \mu^-)$ plane; the light-blue (dark-blue) points have $R < 1.1$ (1.05), while for the orange (red) points $R < 1.1$ (1.05) and $\Omega_{\tilde{\chi}_1^0} h^2 < 0.136$.

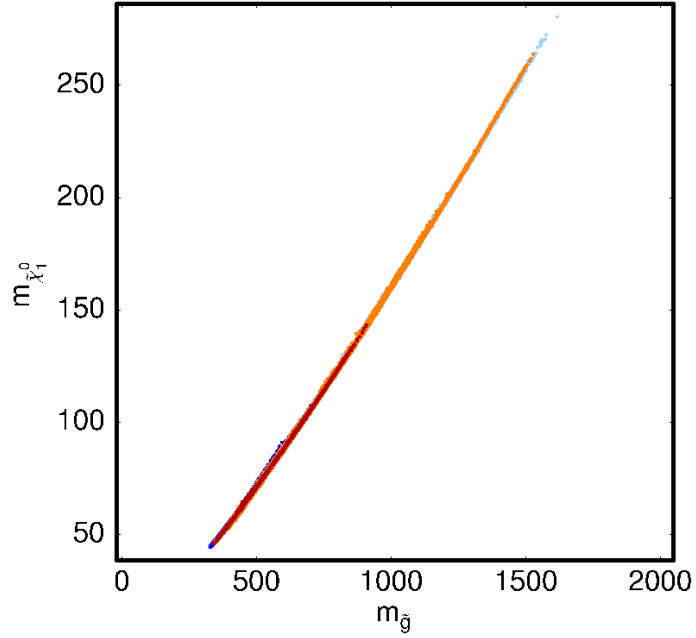


Figure 20: Plot of MCMC results using WSH boundary conditions in the $m_{\tilde{g}}$ vs. $m_{\tilde{\chi}_1^0}$ plane; the light-blue (dark-blue) points have $R < 1.1$ (1.05), while for the orange (red) points $R < 1.1$ (1.05) and $\Omega_{\tilde{\chi}_1^0} h^2 < 0.136$.

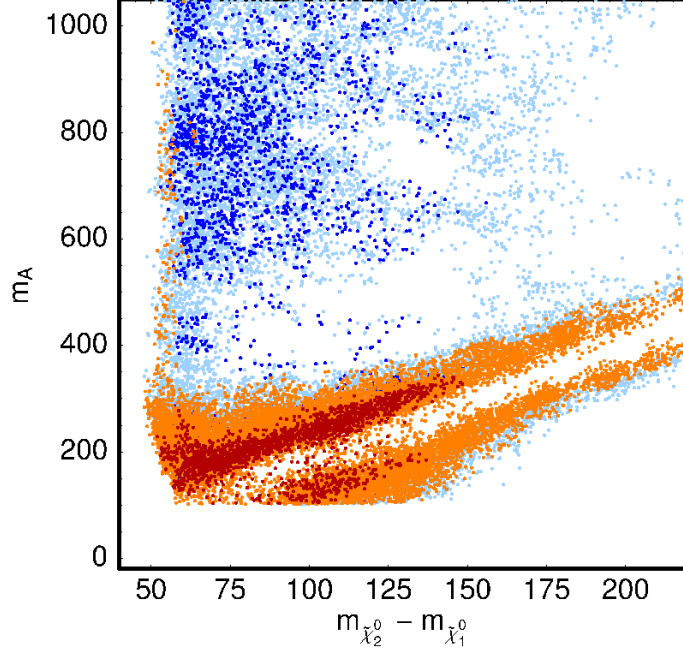


Figure 21: Plot of MCMC results using WSH boundary conditions in the $m_{\tilde{\chi}_2^0} - m_{\tilde{\chi}_1^0}$ vs. m_A plane; the light-blue (dark-blue) points have $R < 1.1$ (1.05), while for the orange (red) points $R < 1.1$ (1.05) and $\Omega_{\tilde{\chi}_1^0} h^2 < 0.136$.

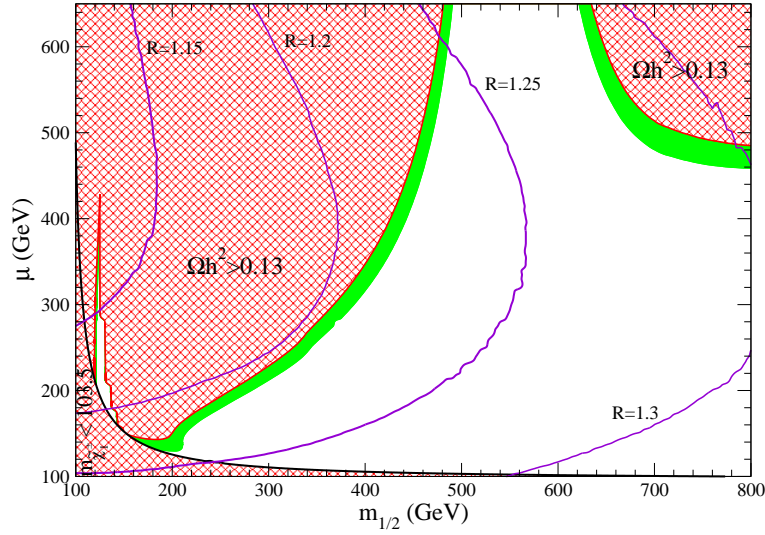


Figure 22: Contours of R and DM-allowed regions in the $m_{1/2}$ vs. μ parameter space for $m_{16} = 3$ TeV, $m_{10}/m_{16} = 1.3$, $A_0/m_{16} = -1.85$, $\Delta m_H = 0.14$, $\tan \beta = 50.9$, $m_A = 500$ GeV and $m_t = 173.9$ GeV, as in Dermisek *et al.*, but using Isajet 7.75 for mass spectra generation.

annihilation at low μ . There is also a light Higgs h -resonance solution at $m_{1/2} \sim 120$ GeV.

A notable feature of Fig. 22 is that over much of the DM-allowed region, the Yukawa unification has $R > 1.2$.⁷ As we move to larger μ values and lower $m_{1/2}$ values, the Yukawa unification gets better and better. Most of the region with $R < 1.15$ is DM-forbidden, save for the upper part of the light h -resonance solution. In fact, now we can see why our compromise solution (point D) works and why it is so hard to find using a top-down approach: only the very narrow upper tip is both DM-allowed, and has a low R value.

4. Yukawa-unified benchmark scenarios and LHC signatures

We have assembled in Table 1 five Yukawa-unified benchmark scenarios that yield the correct relic abundance of dark matter in five different ways. With the LHC turn-on being imminent, it is fruitful to examine what each of these five scenarios implies for new physics signatures.

At the bottom of Table 1 we list $\Omega_{\tilde{\chi}_1^0} h^2$, $BF(b \rightarrow s\gamma)$, $BF(B_s \rightarrow \mu^+ \mu^-)$, Δa_μ and spin-independent neutralino-proton direct DM detection cross section $\sigma(\tilde{\chi}_1^0 p)$. For the first four of these numbers, we list output from IsaReD/Isatools (upper) and micrOMEGAs (lower). While the results for the low-energy constraints agree fairly well, there is almost a factor of 2 difference in the relic density when the neutralino dominantly annihilates through h or A exchange (points A, D, E). This is due to differences in the treatment of the Higgs resonance. For example, IsaReD in Isajet 7.75 uses Yukawa couplings evaluated at scale $Q = \sqrt{m_{\tilde{t}_L} m_{\tilde{t}_R}}$ for annihilation through the A resonance and for evaluation of the heavy Higgs widths, while micrOMEGAs uses an effective Lagrangian approach and $Q = 2m_{\tilde{\chi}_1^0}$.⁸

Point A

Point A of Table 1 is a generic Yukawa-unified model with first and second generation scalar masses ~ 9 TeV, so they essentially decouple from LHC physics. Third generation and heavy Higgs scalars have masses at the 2–3 TeV level, while the lightest charginos, neutralinos and gluinos all have masses in the range 100–400 GeV. Since $\Omega_{\tilde{\chi}_1^0} h^2 \sim 400$, we postulate that the neutralino $\tilde{\chi}_1^0$ is in fact an NLSP, decaying to $\tilde{a}\gamma$ with a lifetime of order 0.03 seconds. In this case, the mean decay distance of a $\tilde{\chi}_1^0$ will be of order 10^4 km. Thus, the $\tilde{\chi}_1^0$ will still escape the LHC detectors, leading to missing energy signatures (although it is conceivable some may decay occasionally within the detector).

The LHC SUSY events will consist of a hard and soft component [44]. The hard component comes from pair production of ~ 400 GeV gluinos. The gluinos decay via 3-body modes dominantly via $\tilde{g} \rightarrow t b \tilde{\chi}_1^\pm$, $b \bar{b} \tilde{\chi}_1^0$ and especially $b \bar{b} \tilde{\chi}_2^0$ [45]. The $\tilde{g}\tilde{g}$ production

⁷Note that although the general features in Fig. 22 here and Fig. 1 of [20] are similar, the latter results were obtained in a top-down fit to low energy observables assuming exact Yukawa unification, which is a different approach than the one followed here. Moreover, there are several important differences in the level of sophistication of the spectrum computations between Ref. [4, 20, 21] and the study presented here. For instance, Ref. [4, 20, 21] has only 1-loop RGE running of the SUSY-breaking parameters, takes sparticle masses to be running masses at scale $Q = M_Z$; ISAJET 7.75 applies full 2-loop running plus 1-loop threshold corrections.

⁸A complete discussion of the details of the calculations in the two programs is beyond the scope of this paper; we refer the interested reader to the respective manuals.

cross section is of order 10^5 fb at LHC, so we might expect 10^7 gluino pair events per 100 fb^{-1} of integrated luminosity. After cascade decays, we expect an assortment of events with high jet and b -jet multiplicity, plus an assortment of isolated leptons. The $\tilde{\chi}_2^0 \rightarrow \tilde{\chi}_1^0 e \bar{e}$ branching fraction is at 2.2% , which should be enough to reconstruct the dilepton mass edge at $m_{\tilde{\chi}_2^0} - m_{\tilde{\chi}_1^0} \simeq 73 \text{ GeV}$. Correct pairing of b -jets and/or b -jets with isolated leptons, plus the total event rate, should allow for an extraction of the gluino mass.

The soft component of signal will come from $\tilde{\chi}_1^+ \tilde{\chi}_1^-$, $\tilde{\chi}_1^\pm \tilde{\chi}_2^0$ and $\tilde{\chi}_1^\pm \tilde{\chi}_1^0$ production. These events will be followed by 3-body decays to various final states, but since the visible components of the signal are much softer than that from gluino pair production, these events will be harder to see above SM background levels. With judicious cuts, the soft component might also be visible at some level (*e.g.* $\tilde{\chi}_1^\pm \tilde{\chi}_2^0 \rightarrow 3\ell + E_T^{\text{miss}}$) [46].

Point B

Point B is the same as point A, except that in this case the gaugino mass M_1 has been raised to 195 GeV so that the $\tilde{\chi}_1^\pm - \tilde{\chi}_1^0$ mass gap shrinks to only 13 GeV. Since μ is quite large, the $\tilde{\chi}_1^0$ remains nearly pure bino-like, but the relic density problem is solved via bino-wino co-annihilation. This case will again give a hard component to the LHC new physics signal from gluino pair production, but this time the $m(\ell^+ \ell^-)$ distribution will have an edge only at 13 GeV. When compared to any gluino mass reconstructions, this would indicate a violation of gaugino mass unification at the GUT scale. In addition, the small $\tilde{\chi}_2^0 - \tilde{\chi}_1^0$ mass gap suppresses 3-body decays such as $\tilde{\chi}_2^0 \rightarrow \tilde{\chi}_1^0 q \bar{q}$ and $\tilde{\chi}_1^0 \ell \bar{\ell}$ relative to any kinematically-allowed 2-body decays such as the loop-induced process $\tilde{\chi}_2^0 \rightarrow \tilde{\chi}_1^0 \gamma$ [47]. Thus, the radiative $\tilde{\chi}_2^0$ decay to photon $\tilde{\chi}_2^0 \rightarrow \tilde{\chi}_1^0 \gamma$ can become large [24]: in this case, it reaches 10%. The final state γ will be somewhat soft if the $\tilde{\chi}_2^0$ is at low velocity. But if $\tilde{\chi}_2^0$ is moving fast as a result of production from cascade decays, then hard, isolated photons should occasionally be present in the SUSY collider events.

Point C

The point C parameters are listed in Table 1. In this case, $m_{16}(1,2)$ has been lowered far below $m_{16}(3)$ so that the first two generations of scalars are degenerate, but with a lower mass than third generation scalars. The Higgs mass splitting leads to a large RGE S -term, which drives \tilde{u}_R and \tilde{c}_R to very low masses $\simeq 98.3 \text{ GeV}$. This is at the edge of LEP2 exclusion. The relic density problem is solved because $\tilde{\chi}_1^0 \tilde{\chi}_1^0 \rightarrow q \bar{q}$ via \tilde{q}_R exchange and neutralino-squark co-annihilation act to reduce the relic density. The cross section for production of two flavors of extremely light squarks is extremely large at LHC. Normally one would expect characteristic dijet+ E_T^{miss} events since $\tilde{q}_R \rightarrow q \tilde{\chi}_1^0$. However, in this case the mass gap $m_{\tilde{u}_R} - m_{\tilde{\chi}_1^0} \sim 18 \text{ GeV}$, so both the jets and E_T^{miss} will be very soft. Gluinos and other squarks will also be produced at large rates, although the $\tilde{g} \rightarrow u \tilde{u}_R$, $c \tilde{c}_R$ decays are dominant. While left-squarks may decay with large rates to $\tilde{\chi}_2^0$ and $\tilde{\chi}_1^\pm$, we note that $\tilde{\chi}_2^0 \rightarrow u \tilde{u}_R$ and $c \tilde{c}_R$ is also large, leading again to relatively soft jet activity. In spite of the soft jet activity, the scenario should be easily seen at LHC, since $\tilde{q}_L \rightarrow q' \tilde{\chi}_1^\pm$ occurs at a large rate, and $\tilde{\chi}_1^\pm \rightarrow e \nu_e \tilde{\chi}_1^0$ occurs at 43% branching fraction (enhanced by the relatively light left-sleptons). This can lead to a large same-sign (SS) dilepton rate from $pp \rightarrow \tilde{u}_L \tilde{u}_L$

parameter	A	B	C	D	E
m_{16}	9202.9	9202.9	5018.8	2976.5	5877.3
$m_{1/2}$	62.5	62.5	160	107.0	113.6
A_0	-19964.5	-19964.5	-10624.2	-6060.3	-12052.6
m_{10}	10966.1	10966.1	6082.1	3787.9	—
$\tan\beta$	49.1	49.1	47.8	49.05	47.4
M_D	3504.4	3504.4	1530.1	1020.8	—
M_1	—	195	—	—	—
$m_{16}(1, 2)$	—	—	603.8	—	—
f_t	0.51	0.51	0.49	0.48	0.49
f_b	0.51	0.51	0.41	0.47	0.49
f_τ	0.52	0.52	0.47	0.52	0.49
μ	4179.8	4186.3	1882.6	331.0	865.3
$m_{\tilde{g}}$	395.6	395.4	495.5	387.7	466.6
$m_{\tilde{u}_L}$	9185.4	9185.4	622.1	2970.8	5863.0
$m_{\tilde{u}_R}$	9104.1	9104.2	98.3	2951.4	5819.2
$m_{\tilde{t}_1}$	2315.1	2310.5	1048.4	434.5	944.7
$m_{\tilde{b}_1}$	2723.1	2714.9	1894.0	849.3	1452.7
$m_{\tilde{e}_L}$	9131.9	9132.0	311.9	2955.8	5833.6
$m_{\tilde{e}_R}$	9323.7	9323.9	891.8	3009.0	5945.8
$m_{\tilde{\chi}_1^\pm}$	128.8	128.8	165.7	105.7	141.3
$m_{\tilde{\chi}_2^0}$	128.6	128.1	165.1	105.1	140.9
$m_{\tilde{\chi}_1^0}$	55.6	115.9	80.2	52.6	65.7
m_A	3273.6	3266.0	1939.9	776.8	177.8
m_h	125.4	125.4	123.2	111.1	113.4
$\Omega_{\tilde{\chi}_1^0} h^2$	423 220	0.09 0.08	0.11 0.11	0.10 0.06	0.15 0.08
$BF(b \rightarrow s\gamma)$	3.0×10^{-4} 3.3×10^{-4}	3.0×10^{-4} 3.3×10^{-4}	6.2×10^{-4} 3.7×10^{-4}	1.9×10^{-4} 4.0×10^{-4}	2.5×10^{-4} 2.2×10^{-4}
Δa_μ	5.0×10^{-12} 5.1×10^{-12}	5.0×10^{-12} 5.0×10^{-12}	3.0×10^{-10} 2.8×10^{-10}	2.2×10^{-10} 2.2×10^{-10}	4.1×10^{-11} 4.1×10^{-11}
$BF(B_s \rightarrow \mu^+ \mu^-)$	5.0×10^{-9} 4.4×10^{-9}	5.0×10^{-9} 4.4×10^{-9}	11.8×10^{-9} 6.9×10^{-9}	5.8×10^{-8} 6.2×10^{-8}	2.0×10^{-5} 2.0×10^{-5}
$\sigma_{sc}(\tilde{\chi}_1^0 p)$ [pb]	1.3×10^{-15}	1.9×10^{-17}	1.5×10^{-6}	2.7×10^{-9}	5.3×10^{-8}

Table 1: Masses and parameters in GeV units for five benchmark Yukawa unified points using Isajet 7.75 and $m_t = 171.0$ GeV. The upper entry for the $\Omega_{\tilde{\chi}_1^0} h^2$ etc. come from IsaReD/Isatools, while the lower entry comes from micrOMEGAs; $\sigma(\tilde{\chi}_1^0 p)$ is computed with Isatools.

production, along with a large asymmetry in $++$ SS dileptons over $--$ SS dileptons (which occur from $\tilde{d}_L \tilde{d}_L$ production). This scenario may also be subject to exclusion by analysis of Fermilab Tevatron data. We further note that point C is naively excluded by direct dark matter search limits. These latter limits depend on an assumed standard local relic density mass and velocity distribution, so that the limits can be avoided if one postulates that we live in a local underdensity of dark matter.

Point D

Point D is an example of a compromise solution, where we allow m_{16} as low as 3 TeV at some expense to Yukawa unification (here, Yukawa unification is good to only $\sim 10\%$) in order to allow for neutralino annihilation through the light Higgs h -resonance (neutralinos can still annihilate through the light h resonance for higher m_{16} values; it is just that the relic density can't be pushed as low as $\Omega_{\tilde{\chi}_1^0} h^2 \sim 0.1$). This scenario is extremely predictive, with gluinos around 350–450 GeV, so again we expect LHC events to be dominated by gluino pair production. As in the case of point A, the $\tilde{g}\tilde{g}$ events will be followed by 3-body decays to b -jet rich final states. A dilepton mass edge at $m_{\tilde{\chi}_2^0} - m_{\tilde{\chi}_1^0} \simeq 53$ GeV should be visible since $\tilde{\chi}_2^0 \rightarrow \tilde{\chi}_1^0 e^+ e^-$ at 3.3% branching fraction. The \tilde{t}_1 weighs only 434 GeV in this case, and \tilde{b}_1 is at 849 GeV, so it may be possible to detect some third generation squark pair production events. The top squark decays to $b\tilde{\chi}_1^\pm$ with a 50% branching fraction, and also has significant branching fractions to $t\tilde{\chi}_1^0$, $t\tilde{\chi}_2^0$ and $b\tilde{\chi}_2^\pm$ final states. The \tilde{b}_1 dominantly decays to $b\tilde{g}$ and $W\tilde{t}_1$ final states. Moreover, the heavy Higgs bosons A^0 , H^0 and H^\pm have masses around 780 GeV and should be detectable at LHC [48].

Point E

Point E is a Yukawa-unified solution that solves the DM abundance problem via neutralino annihilation through a 178 GeV pseudoscalar A resonance. The combination of light A and large $\tan\beta$ leads to a branching fraction $B_s \rightarrow \mu^+ \mu^-$ which is excluded by recent CDF analyses. If we are allowed to somehow ignore this (possibly via other flavor-violating interactions), then the scenario would be at the edge of observability via Tevatron searches for A , $H \rightarrow \tau^+ \tau^-$ and $b\bar{b}$, which at present exclude $m_A \lesssim 170$ GeV [49]. The LHC (and possibly soon also the Tevatron) would easily see the rather light spectrum of Higgs bosons. Gluinos can be somewhat heavier in this case compared to points A and D, ranging to over a TeV. However, in point E as listed, with a 467 GeV gluino, the gluino pair production signatures will be rather similar to those of point A: rich in b -jets, with a visible dilepton mass edge at 75 GeV.

5. Summary and conclusions

In this paper, we have presented a number of new results.

1. First, we verified former results presented in Ref. [18] that Yukawa unified models can be generated with updated Isajet spectra code and an updated value of the top quark mass $m_t = 171$ GeV. Using both random scans and the more efficient MCMC scans, we find that models with excellent Yukawa coupling unification can be generated in the HS model if scalar masses are in the multi-TeV range, while gaugino masses are quite light, and the $\tilde{\chi}_1^\pm$ is slightly above the current LEP2 limit. The models require the Bagger *et al.* boundary conditions if $\mu > 0$ such that $A_0^2 = 2m_{10}^2 = 4m_{16}^2$, and $A_0 < 0$ in our convention. The spectra generated is characterized by three mass scales: multi-TeV first and second generation matter scalars, TeV scale third generation and Higgs scalars and 100–200 GeV light charginos and gluinos of order 350–450 GeV.

The relic density is typically 30–30,000 times above the WMAP measured value. As a solution, we propose *i*). hypothesizing an unstable neutralino $\tilde{\chi}_1^0$ which decays to axino plus photon, *ii*). raising the GUT scale gaugino mass M_1 so that bino-wino co-annihilation reduces the relic density or *iii*). lowering the first/second generation scalar masses relative to the third so that neutralinos can annihilate via light \tilde{q}_R exchange and neutralino-squark co-annihilation. We regard the first of these solutions as the most attractive, and the third is actually susceptible to possible exclusion by analyses of Fermilab Tevatron signals in the case of just two light squarks.

2. Using an MCMC analysis, we find a new class of solutions with $m_{16} \sim 3$ TeV, where neutralinos annihilate through the light higgs h resonance. This low a value of m_{16} typically leads to Yukawa unification at the 5–10% level at best.
3. We find we are able to generate solutions with low μ and low m_A as did the BDR group. The solutions generated by the Isajet code with low μ , low m_A and $m_{16} \sim 3$ TeV tend to have Yukawa unification in the 20% range or greater. We were able to generate a class of solutions with excellent Yukawa unification and m_{16} ranging up to 6 TeV, where the DM problem is solved by neutralino annihilation through a 150–250 GeV A resonance. The combination of large $\tan\beta$ and low m_A gives a $B_s \rightarrow \mu^+\mu^-$ branching fraction at levels beyond those allowed by the CDF collaboration.

We also present a Table of five benchmark solutions suitable for event generation, and for examination of collider signals expected at the LHC from DM-allowed Yukawa-unified SUSY models. Based on this work, we are able to make several predictions, if the Yukawa-unified MSSM is the correct effective field theory between M_{GUT} and M_{weak} . We would expect the following:

- New physics events at the CERN LHC to be dominated by gluino pair production with $m_{\tilde{g}} \sim 350\text{--}450$ GeV. Since $\tan\beta$ is large, the final states are rich in b -jets, and the OS/SF isolated dilepton invariant mass distribution should have a visible edge at $m_{\tilde{\chi}_2^0} - m_{\tilde{\chi}_1^0} \sim 50\text{--}75$ GeV because the $\tilde{\chi}_2^0$ always decays via 3-body modes. Squarks and sleptons are likely to be very heavy, and may decouple from LHC physics signatures.
- We would predict in this scenario that the $(g-2)_\mu$ anomaly is false, since in Yukawa-unified SUSY models with large m_{16} , the SUSY contribution to the muon QED vertex is always highly suppressed.
- While SUSY should be easily visible at the LHC for Yukawa unified models, we would predict a dearth of direct and indirect dark matter detection signals. This is because the typically large values of μ and scalar masses tend to suppress such signals. However, in the CDF-excluded case of point E, the direct and indirect DM signals may be observable. Points C and D also have low but observable direct DM detection rates, since scalars are not too heavy.

Acknowledgments

We thank G. Belanger, A. Belyaev, A. Pukhov and X. Tata for useful comments and discussion, and A. Pukhov for finding a bug in the IsaReD relic density subroutine. This project was initiated during the CERN-TH institute on *LHC–Cosmology Interplay*, where three of us (HB, SK and SS) participated. The hospitality of the CERN TH division is gratefully acknowledged. SS additionally acknowledges the support by TŰBÍTAK grant 106T457 (TBAG-HD 190), enabling her visit to CERN. This research was supported in part by the U.S. Department of Energy grant numbers DE-FG02-97ER41022.

References

- [1] H. Georgi, in *Proceedings of the American Institute of Physics*, edited by C. Carlson (1974); H. Fritzsch and P. Minkowski, *Ann. Phys.* **93**, 193 (1975); M. Gell-Mann, P. Ramond and R. Slansky, *Rev. Mod. Phys.* **50**, 721 (1978). For recent reviews, see R. Mohapatra, hep-ph/9911272 (1999) and S. Raby, in *Rept. Prog. Phys.* **67** (2004) 755.
- [2] Y. Kawamura, *Prog. Theor. Phys.* **105** (2001) 999; G. Altarelli and F. Feruglio, *Phys. Lett. B* **511** (2001) 257; L. Hall and Y. Nomura, *Phys. Rev. D* **64** (2001) 055003; A. Hebecker and J. March-Russell, *Nucl. Phys. B* **613** (2001) 3; A. Kobakhidze, *Phys. Lett. B* **514** (2001) 131.
- [3] P. Minkowski, *Phys. Lett. B* **67** (1977) 421; M. Gell-Mann, P. Ramond and R. Slansky, in *Supergravity, Proceedings of the Workshop*, Stony Brook, NY 1979 (North-Holland, Amsterdam); T. Yanagida, KEK Report No. 79-18, 1979; R. Mohapatra and G. Senjanovic, *Phys. Rev. Lett.* **44** (1980) 912.
- [4] T. Blazek, R. Dermisek and S. Raby, *Phys. Rev. Lett.* **88** (2002) 111804; T. Blazek, R. Dermisek and S. Raby, *Phys. Rev. D* **65** (2002) 115004.
- [5] CDF and D0 collaborations, hep-ph/0703034 (2007).
- [6] B. Ananthanarayan, G. Lazarides and Q. Shafi, *Phys. Rev. D* **44** (1991) 1613 and *Phys. Lett. B* **300** (1993) 245; G. Anderson *et al.* *Phys. Rev. D* **47** (1993) 3702 and *Phys. Rev. D* **49** (1994) 3660; V. Barger, M. Berger and P. Ohmann, *Phys. Rev. D* **49** (1994) 4908; M. Carena, M. Olechowski, S. Pokorski and C. Wagner, Ref. [8]; B. Ananthanarayan, Q. Shafi and X. Wang, *Phys. Rev. D* **50** (1994) 5980; R. Rattazzi and U. Sarid, *Phys. Rev. D* **53** (1996) 1553; T. Blazek, M. Carena, S. Raby and C. Wagner, *Phys. Rev. D* **56** (1997) 6919; T. Blazek and S. Raby, *Phys. Lett. B* **392** (1997) 371; T. Blazek and S. Raby, *Phys. Rev. D* **59** (1999) 095002; T. Blazek, S. Raby and K. Tobe, *Phys. Rev. D* **60** (1999) 113001 and *Phys. Rev. D* **62** (2000) 055001; see also [7].
- [7] S. Profumo, *Phys. Rev. D* **68** (2003) 015006; C. Pallis, *Nucl. Phys. B* **678** (2004) 398; M. Gomez, G. Lazarides and C. Pallis, *Phys. Rev. D* **61** (2000) 123512, *Nucl. Phys. B* **638** (2002) 165 and *Phys. Rev. D* **67** (2003) 097701; U. Chattopadhyay, A. Corsetti and P. Nath, *Phys. Rev. D* **66** (2002) 035003; M. Gomez, T. Ibrahim, P. Nath and S. Skadhauge, *Phys. Rev. D* **72** (2005) 095008.
- [8] R. Hempfling, *Phys. Rev. D* **49** (1994) 6168; L. J. Hall, R. Rattazzi and U. Sarid, *Phys. Rev. D* **50** (1994) 7048; M. Carena *et al.*, *Nucl. Phys. B* **426** (1994) 269; D. Pierce, J. Bagger, K. Matchev and R. Zhang, *Nucl. Phys. B* **491** (1997) 3.

- [9] M. Drees, *Phys. Lett.* **B 181** (1986) 279; J.S. Hagelin and S. Kelley, *Nucl. Phys.* **B 342** (1990) 95; A.E. Faraggi, *et al.*, *Phys. Rev.* **D 45** (1992) 3272; Y. Kawamura and M. Tanaka, *Prog. Theor. Phys.* **91** (1994) 949; Y. Kawamura, *et al.*, *Phys. Lett.* **B 324** (1994) 52 and *Phys. Rev.* **D 51** (1995) 1337; N. Polonsky and A. Pomarol, *Phys. Rev.* **D 51** (1994) 6532; H.-C. Cheng and L.J. Hall, *Phys. Rev.* **D 51** (1995) 5289; C. Kolda and S.P. Martin, *Phys. Rev.* **D 53** (1996) 3871.
- [10] H. Baer, M. Diaz, J. Ferrandis and X. Tata, *Phys. Rev.* **D 61** (2000) 111701.
- [11] Isajet, by F. Paige, S. Protopopescu, H. Baer and X. Tata, [hep-ph/0312045](#).
- [12] H. Baer, M. Brhlik, M. Diaz, J. Ferrandis, P. Mercadante, P. Quintana and X. Tata, *Phys. Rev.* **D 63** (2001) 015007.
- [13] H. Baer and J. Ferrandis, *Phys. Rev. Lett.* **87** (2001) 211803.
- [14] J. Feng, C. Kolda and N. Polonsky, *Nucl. Phys.* **B 546** (1999) 3; J. Bagger, J. Feng and N. Polonsky, *Nucl. Phys.* **B 563** (1999) 3; J. Bagger, J. Feng, N. Polonsky and R. Zhang, *Phys. Lett.* **B 473** (2000) 264.
- [15] H. Baer, P. Mercadante and X. Tata, *Phys. Lett.* **B 475** (2000) 289; H. Baer, C. Balazs, M. Brhlik, P. Mercadante, X. Tata and Y. Wang, *Phys. Rev.* **D 64** (2001) 015002.
- [16] K. Tobe and J. D. Wells, *Nucl. Phys.* **B 663** (2003) 123.
- [17] H. Baer, M. Diaz, P. Quintana and X. Tata, *J. High Energy Phys.* **0004** (2000) 016.
- [18] D. Auto, H. Baer, C. Balazs, A. Belyaev, J. Ferrandis and X. Tata, *J. High Energy Phys.* **0306** (2003) 023.
- [19] D. N. Spergel *et al.* (WMAP Collaboration), [astro-ph/0603449](#) (2006).
- [20] R. Dermisek, S. Raby, L. Roszkowski and R. Ruiz de Austri, *J. High Energy Phys.* **0304** (2003) 037.
- [21] R. Dermisek, S. Raby, L. Roszkowski and R. Ruiz de Austri, *J. High Energy Phys.* **0509** (2005) 029.
- [22] D. Auto, H. Baer, A. Belyaev and T. Krupovnickas, *J. High Energy Phys.* **0410** (2004) 066.
- [23] H. Baer, A. Belyaev, T. Krupovnickas and A. Mustafayev, *J. High Energy Phys.* **0406** (2004) 044.
- [24] H. Baer, T. Krupovnickas, A. Mustafayev, E. K. Park, S. Profumo and X. Tata, *J. High Energy Phys.* **0512** (2005) 011.
- [25] H. Baer, J. Ferrandis, S. Kraml and W. Porod, *Phys. Rev.* **D 73** (2006) 015010.
- [26] H. Baer, J. Ferrandis, K. melnikov and X. Tata, *Phys. Rev.* **D 66** (2002) 074007.
- [27] S. Martin and M. Vaughn, *Phys. Rev.* **D 50** (1994) 2282.
- [28] H. Haber and R. Hempfling, *Phys. Rev.* **D 48** (1993) 4280.
- [29] B.C. Allanach, S. Kraml and W. Porod, *J. High Energy Phys.* **03** (2003) 016; G. Belanger, S. Kraml and A. Pukhov, *Phys. Rev.* **D 72** (2005) 015003; S. Kraml and S. Sekmen in: *Physics at TeV Colliders 2007, BSM working group report*, in prep..

- [30] H. Baer, K. Hagiwara and X. Tata, *Phys. Rev. D* **35** (1987) 1598; H. Baer, D. Dzialo-Karatas and X. Tata, *Phys. Rev. D* **42** (1990) 2259; H. Baer, C. Kao and X. Tata, *Phys. Rev. D* **48** (1993) 5175; H. Baer, C. H. Chen, F. Paige and X. Tata, *Phys. Rev. D* **50** (1994) 4508; I. Hinchliffe *et al.*, *Phys. Rev. D* **55** (1997) 5520 and *Phys. Rev. D* **60** (1999) 095002; H. Bachacou, I. Hinchliffe and F. Paige, *Phys. Rev. D* **62** (2000) 015009; Atlas Collaboration, LHCC 99-14/15; C. Lester, M. Parker and M. White, *J. High Energy Phys.* **0601** (2006) 080.
- [31] See I. Hinchliffe *et al.*, Ref. [30].
- [32] J. Feng, A. Rajaraman and F. Takayama, *Phys. Rev. Lett.* **91** (2003) 011302 and *Phys. Rev. D* **68** (2003) 063504.
- [33] L. Covi, H. B. Kim, J. E. Kim and L. Roszkowski, *J. High Energy Phys.* **0105** (2001) 033.
- [34] K. Jedamzik, M. Lemoine and G. Moulta, *JCAP***0607** (2006) 010.
- [35] L. Covi, J. E. Kim and L. Roszkowski, *Phys. Rev. Lett.* **82** (1999) 4180.
- [36] A. Birkedal-Hansen and B. Nelson, *Phys. Rev. D* **64** (2001) 015008 and *Phys. Rev. D* **67** (2003) 095006; H. Baer, A. Mustafayev, E. K. Park and S. Profumo, *J. High Energy Phys.* **0507** (2005) 046.
- [37] F. Gabbiani, E. Gabrielli, A. Masiero and L. Silvestrini, *Nucl. Phys. B* **477** (1996) 321.
- [38] A. A. Markov, *Extension of the limit theorems of probability theory to a sum of variables connected in a chain*, reprinted in Appendix B of: R. Howard, *Dynamic Probabilistic Systems, volume 1: Markov Chains*, John Wiley and Sons, 1971.
- [39] N. Metropolis, A.W. Rosenbluth, M.N. Rosenbluth, A.H. Teller, and E. Teller, *Journal of Chemical Physics*, 21(6):1087-1092, 1953; W.K. Hastings, *Biometrika*, 57(1):97-109, 1970; see also C.G. Lester, M.A. Parker, M.J. White, *J. High Energy Phys.* **0601** (2006) 080.
- [40] J. Hamann, S. Hannestad, M. S. Sloth, Y. Y. Y. Wong, *Phys. Rev. D* **75** (2007) 023522.
- [41] G. Belanger, F. Boudjema, A. Pukhov and A. Semenov, *Comput. Phys. Commun.* **174** (2006) 577; *Comput. Phys. Commun.* **176** (2007) 367.
- [42] K. Babu and C. Kolda, *Phys. Rev. Lett.* **84** (2000) 228; A. Dedes, H. Dreiner and U. Nierste, *Phys. Rev. Lett.* **87** (2001) 251804; J. K. Mizukoshi, X. Tata and Y. Wang, *Phys. Rev. D* **66** (2002) 115003;
- [43] K. Tollefson, talk given at *Lepton Photon 07*, August 2007, Daegu, Korea; see http://chep.knu.ac.kr/lp07/htm/S4/S04_14.pdf.
- [44] H. Baer, V. Barger, G. Shaughnessy, H. Summy and L.-t. Wang, *Phys. Rev. D* **75** (2007) 095010.
- [45] H. Baer, C. H. Chen, M. Drees, F. Paige and X. Tata, *Phys. Rev. Lett.* **79** (1997) 986.
- [46] H. Baer, C. H. Chen, F. Paige and X. Tata, *Phys. Rev. D* **50** (1994) 4508.
- [47] H. Komatsu and H. Kubo, *Phys. Lett. B* **157** (1985) 90 and *Nucl. Phys. B* **263** (1986) 265; H. E. Haber, G. Kane and M. Quiros, *Phys. Lett. B* **160** (1985) 297 and *Nucl. Phys. B* **273** (1986) 333; G. Gamberini, *Z. Physik C* **30** (1986) 605; R. Barbieri, G. Gamberini, G. F. Giudice and G. Ridolfi, *Nucl. Phys. B* **296** (1988) 75; H. E. Haber and D. Wyler, *Nucl. Phys. B* **323** (1989) 267; S. Ambrosanio and B. Mele, *Phys. Rev. D* **53** (1996) 2541 and *Phys. Rev. D* **55** (1997) 1399 [Erratum-ibid. **D56**, 3157 (1997)]; H. Baer and T. Krupovnickas, *J. High Energy Phys.* **0209** (2002) 038.

- [48] ATLAS Collaboration, LHCC 99-14/15 (1999); CMS Collaboration, *J. Phys.* **G** **34** (2007) 1.
- [49] A. Abulencia *et al.* (CDF Collaboration), *Phys. Rev. Lett.* **96** (2006) 011802; V. Abazov *et al.* (D0 Collaboration), *Phys. Rev. Lett.* **97** (2006) 121802.